structure and topological metrics change during the normal course of development [18–21], hub organization is stable from adolescence to young adulthood in neurotypical individuals [17], providing the notion that hub organization may serve as a functional backbone of the human brain. On the other hand, there is evidence for atypical neurodevelopment during adolescence in individuals with ASC [22], which raises the possibility that significant changes in hub organization occur between adolescence and adulthood.

A number of studies have applied graph-theoretical analysis to clinical populations, including patients with schizophrenia [23–27], major depressive disorder [28], and other disorders [29,30]. Although the graph-theoretical approaches are now being applied to studies on different aspects of the ASC brain (e.g., white matter connectivity and electrophysiological connectivity) [31–35], only a few have applied graph-theoretical analysis to rs-fMRI data of this disorder [36–39]. Rudie et al. [39] recently described disrupted local segregation and enhanced global integration in adolescents with ASC compared to neurotypical counterparts, while Barttfeld et al. [36] have reported that changes in the small-worldness measure occurring at shifts between different cognitive states show opposite patterns in patients with ASC and controls. However, basic questions regarding global network organization and possible alterations of "hubness" in adults with ASC have not been fully addressed.

Growing evidence suggests that people with ASC exhibit atypical neurodevelopmental process at least persisting immediately before adulthood [22,40–42]. For instance, individuals with ASC show brain over-growth in early childhood, followed by a period with an accelerated rate of decline in brain size from adolescence to middle age [42]. In addition, the developmental trajectories of subcortical regions (e.g., putamen and caudate) are known to be different in individuals with ASC relative to normal controls [43]. Furthermore, functional abnormalities of ASC vary with age [44], as corroborated by a meta-analysis revealing that the neural anomalies in adults with ASC differed significantly from those in children [45]. Therefore, in addition to the previous pediatric data, it is important to investigate the topological properties of the brain network in adults with ASC to complement the time-course of changes in topological properties from adolescence to adulthood.

The present study applied a graph-theoretical analysis to rs-fMRI data and compared the local and global topological properties of the brain network of adults with ASC to those of age- and gender-matched controls. In particular, we focused on the analysis of hub organization using local metrics and examined whether the order of node importance is altered in the autistic brain network. Since previous findings suggested that adults with ASC showed under-connectivity when compared to normal controls [2], we hypothesized that: 1) adults with ASC would show aberrant network organization as quantified by several global metrics, such as decreases in clustering coefficient and characteristic path length; 2) local network metrics would be altered in several regions for which activation and/or connectivity have been shown to be abnormal in ASC (e.g., the anterior cingulate cortex); 3) several topological properties altered in ASC would be linked with the autistic trait as assessed by the Autism-Spectrum Quotient (AQ) test [46]; and 4) given the altered pattern of behavioral strengths and weaknesses in ASC, participants with ASC would exhibit significantly altered hub organization and alterations of "hubness" in nodes (e.g., superior temporal sulcus) responsible for a broad range of dysfunctions in ASC.

Materials and Methods

1. Participants

Forty-six adults with ASC were recruited from outpatient units of the Karasuyama Hospital, Tokyo, Japan. The inclusion criteria were: (1) age between 18 and 55 years and (2) a formal diagnosis of pervasive developmental disorder (PDD) based on the Diagnostic and Statistical Manual of Mental Disorders, Fourth Edition (DSM-IV). Exclusion criteria included a history of electroconvulsive therapy, alcohol or other drug abuse or dependence, or any neurological illness affecting the central nervous system. PDD was diagnosed by a team of three experienced psychiatrists and one clinical psychologist, based on two detailed interviews with the patients regarding their development and behavior from infancy through adolescence and family history. The interviews were conducted independently by one of the psychiatrists and the clinical psychologist in the team. The patients were also asked to bring along suitable informants who had known them in early childhood. The psychiatrist gave the final diagnosis, after consultation with the other psychiatrist and the clinical psychologist, a process requiring approximately three hours. This team confirmed that none of the participants met the DSM-IV criteria for any other psychiatric disorder. Although there were some individuals with ASC who showed some levels of anxiety, mood, or attention deficit and hyperactivity disorders, the severity of the problems did not meet the diagnostic criteria for other mental disorders.

A total of 46 normal controls (NCs) were recruited by advertisements and acquaintances. None of the NCs reported any severe medical problem or history of any neurological or psychiatric problems. Moreover, the Mini-International Neuropsychiatric Interview was used to confirm that none of the NCs met the diagnostic criteria for any psychiatric disorder.

The intelligence quotient (IQ) scores of participants with ASC were evaluated using either the Wechsler Adult Intelligence Scale-Third Edition (WAIS-III) or the WAIS-Revised (WAIS-R), while those of NCs were estimated using a Japanese version of the National Adult Reading Test (JART) [47]. Based on the National Adult Reading Test (NART) for English-speaking population [48], the JART has been developed to estimate the IQ of a Japanese subject by scoring his or her reading ability of 25 words printed in Kanji (adopted logographic Chinese characters). It has been widely used in Japanese clinical studies both for normal and patient groups [49,50]. Every participant with ASC was considered as being high-functioning, because his or her full-scale IQ score was higher than 80. Although the IQ score was missing for one male participant with ASC, he was also regarded as being high-functioning, because his predicted IQ was 114 based on the JART. Handedness was assessed using the Edinburgh Handedness Inventory [51]. Furthermore, participants completed the Japanese version of the Autism-Spectrum Quotient (AQ) test [46,52]. All of the participants of this study had normal or corrected-to-normal vision. Within the ASC group, 14 of the 46 participants were using either one or more of the following medications: antidepressants (9 patients), hypnotic drugs (9 patients), anti-anxiety drugs (8 patients), antipsychotic drugs (6 patients), and antiepileptic drugs (3 patients). The summary of participant demographic information can be found in Table 1.

The Ethics Committee of the Faculty of Medicine of Showa University approved all of the procedures used in this study, including the method of obtaining consent, in accordance with the Declaration of Helsinki. Written informed consent was obtained from participants after fully explaining the purpose of this study. Since all participants were high-functioning (IQ>80) adults

Table 1. Demographics and rating scale of the participants.

	NC		ASC		Statistics		
	Mean ± s.d.	Range	*N*	Mean ± s.d.	Range	*N*	*df*	*p*-value
Sample size			46 (7 female)			46 (7 female)		
Age (years)	32.02±7.94	19–50	46	31.11±8.14	19–51	46	90	0.68
Handedness	80.68±49.40	−100–100	41	69.49±63.59	−100–100	45	84	0.37
Estimated IQ	107.59±8.64	87.46–119.8	44	105.8±14.12	83–134	45	87	0.47
AQ score	15.08±5.27	8–30	38	36.20±5.63	24–47	46	82	<0.001

NC: normal control, ASC: autism spectrum condition, s.d.: standard deviation, *N*: the sample size for each of demographic information, AQ: Autism Spectrum Quotient.

doi:10.1371/journal.pone.0094115.t001

without any other comorbidities, they were able to fully understand the content and nature of this study. Guardians' verbal consent was neither documented nor recorded because every patient was judged to possess the full ability to give consent on his or her own by his or her primary doctor (TY, WH, MN, or NK). Any concern regarding the possibility of reduced capacity to consent on his or her own was not voiced by either the ethics committee or patients' primary doctors. Every participant was assigned an arbitrary identification number for this study, so that all the data, including imaging and demographic data, could be analyzed anonymously. The data were stored locally, at a single location in the Department of Psychiatry, Showa University. In accordance with the obtained written informed consent, the data were only available for use by our research group.

2. MRI Data Acquisition

All MRI data were acquired using a 1.5-Tesla GE Signa system (General Electric, Milwaukee, WI, USA) with a phased-array whole-head coil. The functional images were acquired using a gradient echo-planar imaging sequence (in-plane resolution: 3.4375×3.4375 mm, echo time (TE): 40 ms, repetition time (TR): 2000 ms, flip angle: 90°, slice thickness: 4 mm with a 1-mm slice gap [11,53], matrix size: 64×64, 27 axial slices). Two hundred and eight volumes were acquired in a single run. The first four volumes were discarded to allow for T1 equilibration. In addition, a high-resolution T1-weighted spoiled gradient recalled (SPGR) 3D MRI image was collected (in-plane resolution: 0.9375×0.9375 mm, 1.4 mm slice thickness, TR: 25 ms, TE: 9.2 ms, matrix size: 256×256, 128 sagittal slices). Each participant was instructed to lie relaxed in the scanner and to remain as still as possible with his or her eyes closed, yet to stay awake in the dim scanner room.

3. Data Preprocessing

SPM8 software (http://www.fil.ion.ucl.ac.uk/spm/software/spm8/) was used to perform fMRI data preprocessing. First, slice timing and head motion were corrected. No participant was excluded due to excessive motion (>±2 mm translation and > ±2° rotation from the first volume in any axis). We also evaluated the amount of translation and rotation of the head during the scanning of each subject according to the following equation [54]:

$$\text{Translation/Rotation} = \frac{1}{T}\sum_{t=2}^{T}\sqrt{\Delta x_t^2 + \Delta y_t^2 + \Delta z_t^2},$$

where T is the number of volumes (i.e., $T = 204$ in this study); variables x, y, and z stand for translation or rotation values in each of the three axes; and Δx_i is the difference between x_i and x_{i-1} in the x-axis. The amount of head motion was comparable between the two groups in both translation (NC: 0.049±0.026 (mean ± standard deviation); ASC: 0.043±0.024; t-test: $t = 1.140$, $p = 0.257$) and rotation (NC: 0.037±0.014; ASC: 0.034±0.014; t-test: $t = 1.016$, $p = 0.312$). For each participant, a T1-weighted SPGR image was realigned along the mid-sagittal anterior-posterior commissure line, and then the realigned T1-weighted image was segmented and reconstructed in order to generate a skull-tripped T1-weighted image. The realigned fMRI images were co-registered to the skull-stripped T1-weighted image; the fMRI images were then spatially normalized to the standard Montreal Neurological Institute (MNI) template, and were resampled to a resolution of 3×3×3 mm. Finally, the images were spatially smoothed using a 6-mm full-width half-maximum Gaussian kernel.

4. Network Construction

4.1. Definitions of nodes and edges. Functional brain networks consist of nodes and edges. In this study, nodes and edges corresponded to regions of interest (ROIs) and functional connectivity between all possible pairs of the ROIs, respectively. We used the MNI coordinates of 160 brain regions provided by a previous meta-analytic study [55], and constructed a ROI consisting of voxels within a 5-mm radius sphere around the coordinate for each node. The mean time-series was extracted from each ROI, and then artifactual components were removed from the mean time-series using the CompCor method [56] implemented in the Functional Connectivity Toolbox (http://www.nitrc.org/projects/conn/). Briefly, this method first identifies five principal components associated with physiological signals from the segmented white matter and cerebrospinal fluid regions in each participant, and then regresses out those time-series, together with those associated with six head motion parameters and their temporal derivatives from the extracted mean time-series in each ROI. In this study, no global signal regression was performed to avoid the risk of yielding spurious negative correlations [57].

To reduce systematic biases in functional connectivity induced by sub-millimeter head motions during the scan [58,59], we adopted the "scrubbing" method together with a frame-wise displacement (FD) threshold of 0.5 mm and a band-pass filter (0.009–0.08 Hz) [58] (see Text S1 and Figure S1 for details and the effect of scrubbing). We confirmed that the mean FD was comparable between the two groups (NC: 0.1153±0.0423; ASC: 0.1034±0.0466; $t=1.28$, $p=0.201$). After these scrubbing steps, the number of retained volumes was comparable between the groups (NC: 203.17±1.51 volumes; ASC; 202.93±2.51 volumes; t-test: $t=0.554$, $p=0.581$), and each group retained approximately 99.5% of their original volumes. For measuring functional connectivity, correlation coefficients between all possible pairs of the ROIs were then calculated, which resulted in a 160×160 correlation matrix for each participant. Finally, each correlation matrix was transformed into an adjacency matrix by applying a predefined threshold (see next section), where the i-th and the j-th nodes were connected if the (i,j)-th element of the adjacency matrix is equal to one. See Text S2 for functional connectivity analysis.

4.2. Threshold selection. A binary undirected graph was constructed by applying a correlation threshold, ranging from zero to one, to each element of the correlation matrix; however, applying a single common threshold across all participants yields a different number of edges and nodes, which in turn may induce spurious between-group differences in network topology [60]. To avoid this problem, the sparsity-based threshold, S, the ratio of the number of existing edges to the maximum possible number of edges in a graph (= 12720), was employed [26,28].

The range of sparsity-based thresholds S was determined using the following procedures. First, we identified the minimum number of positive elements in the correlation matrix to determine the maximum sparsity (i.e., higher limit) for each participant, and then identified the minimum sparsity (i.e., lower limit), in which there was no fragmentation of the graph into several components for each participant. All graphs satisfied the property of the small-world network (i.e., the small-worldness scalar σ is greater than one). See the following section for a description of the small-worldness scalar. The range of sparsity was determined as $19.50\% \leq S \leq 48.43\%$. Over this range, we repeatedly calculated the global and local network metrics of interest (see next section) with an interval of 0.63% (47 steps).

5. Network Metrics

To assess topological properties of graphs, local and global metrics were calculated on a graph at each of the 47 sparsity levels. Brief descriptions of the metrics used in this study are listed in Table S1. More detailed definitions and descriptions of the metrics can be found in a recent review [61]. For each node, we calculated the three local metrics: degree k, betweenness b, and nodal efficiency e. For global metrics, we calculated global efficiency E_{glob}, local efficiency E_{loc}, and assortativity r. In addition to those global metrics, we computed the small-world parameters [10], including clustering coefficient C, characteristic path length L, normalized clustering coefficient γ, normalized characteristic path length λ, and small-worldness scalar σ. Small-world network should satisfy the conditions of $\gamma>1$ and $\lambda \approx 1$ (i.e., $\sigma>1$). Although we calculated all the above-mentioned global metrics, we reported mainly on r, C, L, and σ because some metrics bore a certain relationship (i.e., proportional or inverse) to other metrics. For example, clustering coefficient C bears a proportional relationship to local efficiency E_{loc}, while characteristic path length L is inversely proportional to global efficiency E_{glob} [62]. All metrics were calculated using the Brain Connectivity Toolbox (http://www.brain-connectivity-toolbox.net/).

While each of the metrics is highly dependent upon the threshold, there is no standard threshold currently accepted for the network construction. To avoid arbitrariness in network thresholding, we calculated the area under the curve (AUC) of each metric. The AUC provides an integrated scalar value representing the metric under investigation across the examined range of sparsity. The robustness of the AUC analysis for metrics has been demonstrated in previous studies [28,63].

6. Hubness

Hubs are often identified using degree k, betweenness b, and nodal efficiency e. High-degree nodes can be considered as centers for information integration; those with high betweenness may serve as way stations for network traffic, and those with high nodal efficiency have superior information propagation ability and hence contribute to efficient information flow [13,64]. In this study, hubs were defined as nodes with a k, b, or e value more than one standard deviation above the mean of all the nodes in the network [15].

7. Hub Disruption Index

Differences in local metrics are usually evaluated at each nodal level rather than at the network level. The hub disruption index is a useful metric for summarizing and visualizing the pattern of nodal abnormalities in a clinical group compared to a neurotypical group [65].

We calculated the hub disruption index, κ, in order to evaluate alteration in network topology in each individual brain, with reference to the normative network topology of the NC group. For each node in the network, we first subtracted the mean local metric (e.g., degree) in the NC group from the normalized degree in a participant, and then plotted the value against the mean of the NC group. We estimated slope using linear regression analysis, and defined the obtained slope as κ. When the resulting data are scattered along a horizontal line ($\kappa=0$), there is no disruption in that participant. In contrast, data scattered along a negatively sloping line ($\kappa<0$) indicates some disruption in that participant. For instance, in comatose patients, high-degree nodes in the NC group showed a significant reduction of degree in the patients, while some low-degree nodes in the NC group showed a significant increase of degree in the patients, resulting in a significant negative slope for the patient group [65]. We expected

that the ASC group would show some altered patterns in their local metrics. The hub disruption index was calculated separately for the three local metrics of degree κ_D, betweenness κ_B, and nodal efficiency κ_E. Of note, the calculation of the hub disruption index was performed on the normalized AUC metric of each local metric.

8. Statistical Analysis

8.1. Differences in network metrics. For between-group comparison of each of the metrics described above, permutation-based nonparametric tests with 5000 permutations were performed on the AUC of that metric, including age and gender as nuisance covariates. For each measure over the range of thresholds, two-sample two-tailed *t*-tests were performed in order to evaluate between-group differences, and a false discovery rate (FDR) correction was used for multiple comparisons [66].

8.2. Reproducibility of hubs. As described previously, hubs were identified using a predefined threshold for degree k, betweenness b, or nodal efficiency e. Although several studies have identified functional hubs according to this manner, it is difficult to confirm whether or not those hubs are reproducible. In this study, we evaluated reproducibility using the bootstrapping method [67]. Within each group, each of the local metrics was resampled, and then hubs were identified using the resampled data and a predefined threshold. This procedure was repeated 10,000 times, and then we counted the occurrence frequency of hubness at each node. Finally, we computed the summation of the frequencies across all the three metrics at each node as a score of hubness of the node. We regarded a node as a functional hub if its score was higher than 2.1 (i.e., the frequency at each local metric was greater than 0.7 on average).

8.3. Relationship between network metrics and AQ score. If a between-group difference in any of the global metrics or hub disruption indices was observed, we further investigated the relationship between the metric and the AQ score using a partial correlation analysis, with age and gender as controlling variables. For the local metrics, we repeated the partial correlation analysis only on nodes where significant group difference was found on all the three local metrics without correction for multiple comparisons, to minimize the problem of multiple comparisons.

Results

1. Global Network Metrics

The global metrics of assortativity r, clustering coefficient C, characteristic path length L, and small-worldness σ in each group are depicted in Figure 1. Figures 1A to D represent the mean and standard error of these metrics, calculated at each sparsity level. For other global metrics (i.e., global efficiency E_{glob}, local efficiency E_{loc}, normalized clustering coefficient γ, and normalized characteristic path length λ), see Figures S2 and S3. As shown in Figure 1D and Figures S2C and S2D, the networks of both the NC and ASC groups exhibited the small-world properties ($\gamma>1$, $\lambda \approx 1$, and $\sigma>1$) over the entire range of thresholds. The AUC analyses revealed that, while σ was comparable between the groups, r, C, and L were significantly lower in participants with ASC than in NCs (r: $p=0.013$; C: $p=0.014$; L: $p=0.002$) (Figure 2).

2. Local Network Metrics

Group comparisons of the local metrics are shown in Figure 3 and Table S2. In total, we identified 28 nodes showing a significant group difference ($p<0.05$) in at least 1 metric: 5 in the fronto-parietal (FP) network, 6 in the cingulo-opercular (CO) network, 4 in the default-mode (DEF) network, 5 in the occipital (OC) network, 5 in the sensorimotor (SE) network, and 3 in the cerebellar (CER) network. While increased local metrics in the ASC group were mainly observed in the OC network, reductions were found in the FP and CO networks (Table 2). Notably, all three local metrics were significantly decreased at the left anterior cingulate cortex (ACC) [−2, 30, 27] and right superior temporal sulcus (STS) [52, −15, −13] and increased at the supplementary motor area (SMA) [0, −1, 52] in the ASC group.

3. Hubness

Hubs were identified using each of the normalized local metrics and the bootstrapping method described previously. For the sake of simplicity, a node is referred to as a *common* hub if that node was identified as a hub in both groups, and a node is referred to as a *group-specific* hub if that node was identified as a hub in only one group.

In total, we identified 15 nodes that showed *common* or *group-specific* hub properties in the whole brain (Figure 4 and Table 3). Among those nodes, we found that five NC-specific hubs were in the right hemisphere (e.g., the bilateral STS, right dorsolateral prefrontal cortex (dlPFC), and precuneus), six ASC-specific hubs located bilaterally in the brain (e.g., the bilateral Heschl's gyri and bilateral precentral gyri), and four common hubs located mainly in the frontal and parietal regions (the bilateral temporoparietal junction (TPJ), right inferior frontal gyrus (IFG) pars opercularis, and precentral/IFG). For functional hubs identified based on each local metric, see Figures S4, S5, and S6. The existence of group-specific hubs indicates an alteration of hub organization in the ASC group.

4. Hub Disruption Indices

Consistent with the possibility of altered hub organization in ASC, the hub disruption index κ exhibited significant negative values for the ASC group in all three metrics (κ_D: $p=0.007$; κ_B: $p<0.001$; κ_E: $p=0.006$) (Figures 5A to C). For instance, the right STS consistently held hub properties across all three local metrics in the NC group, and its averaged network topology in the ASC group was smaller than the normative network topology of the NC group; on the other hand, the right ventrolateral PFC (vlPFC) [46, 39, −15] consistently held hub properties across all three local metrics in the ASC group, and its averaged network topology in the ASC group was greater than the reference calculated from the NC group (Figures 5D to F).

5. Relationship between Altered Network Topology and the AQ Score

No significant correlation was found between the AQ score and any of the global metrics or any of the hub disruption indices. For the local metrics, we only focused on nodes that showed significant alterations in all three local metrics. Thus, the left ACC, SMA, and right STS were selected as candidates for further partial correlation analyses. As shown in Figure 6, we found significant correlations between the AQ score and two of the local metrics of the ACC (k: $r=-0.291$, $p=0.049$; e: $r=-0.298$, $p=0.044$), suggesting that the severity of autistic traits may be reflected in the alterations of nodal metrics.

Discussion

This study examined the topological properties of the resting-state functional brain network in participants with ASC using a graph-theoretical analysis. Participants with ASC showed significant decreases in clustering coefficient C and characteristic path length L, which is consistent with previous findings in adolescents

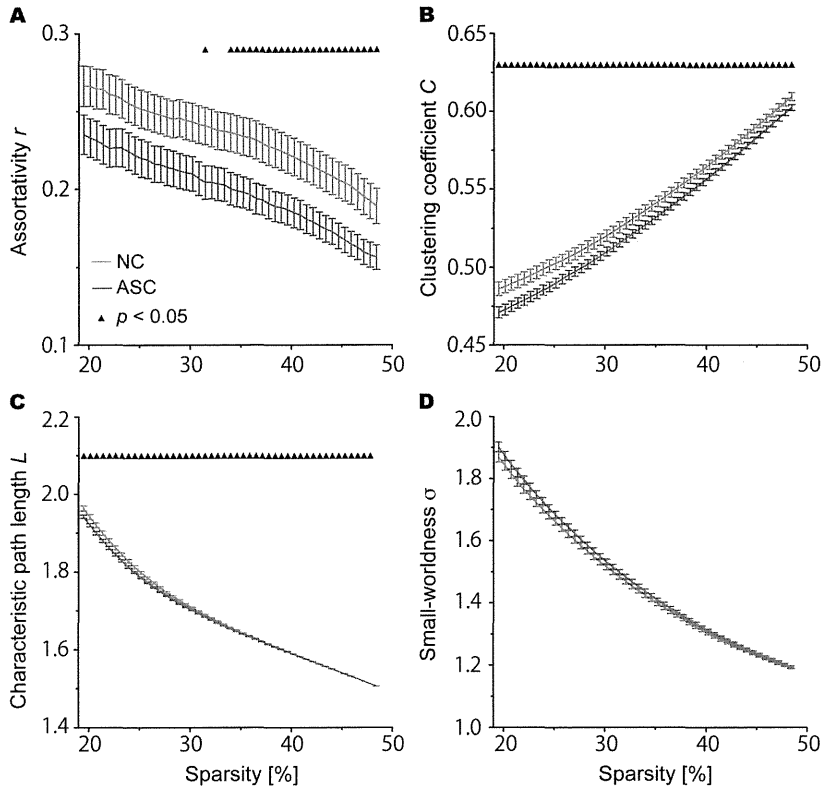

Figure 1. Global metrics of the assortativity, *r*; clustering coefficient, *C*; characteristic path length, *L*; and small-worldness scalar, σ as functions of the sparsity threshold. The ASC group (red line) exhibited lower *C* (B) and *L* (C) than the NC group (blue) over the range of sparsity thresholds ($p<0.05$, FDR corrected), while σ was comparable between groups (D). In addition, *r* was significantly lower in participants with ASC than in NCs over 33.9% of sparsity threshold values (A). The error bar indicates the standard error of the mean (SEM).
doi:10.1371/journal.pone.0094115.g001

with ASC [39]. Furthermore, reduced assortativity was found in ASC, implying that high-degree nodes tended to connect with low-degree nodes to a greater degree in the ASC brain than in the neurotypical brain. These findings are consistent with the view

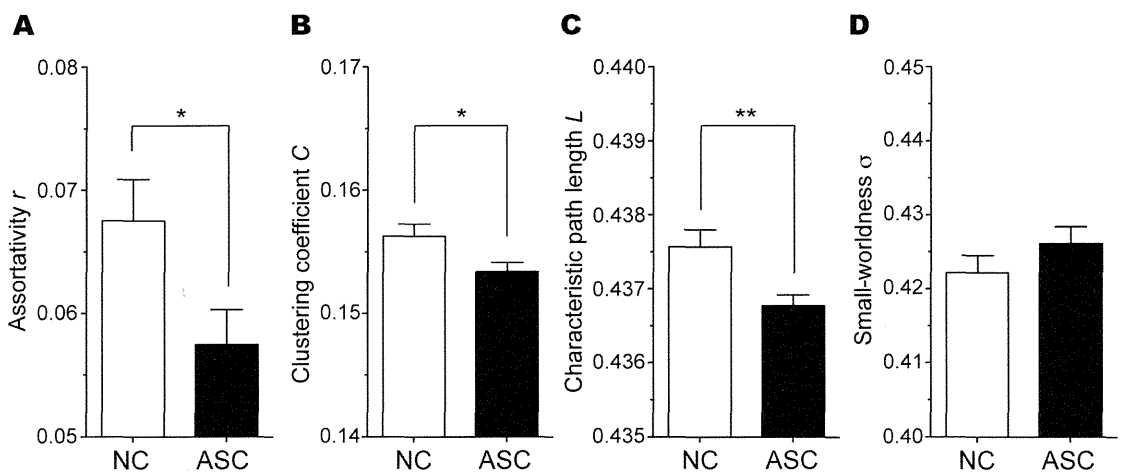

Figure 2. Between-group differences in the AUC values of assortativity, *r*; clustering coefficient, *C*; characteristic path length, *L*; and small-worldness scalar, σ. In the AUC analyses, participants in the ASC group (black) also showed significantly lower *r* ($p=0.013$) (A), *C* ($p=0.014$) (B), and *L* ($p=0.002$) (C) than those in the NC group (white), whereas there were no significant differences in the small-worldness scalar σ (D) between the groups. The error bar indicates the standard error of the mean (SEM). Significance levels are represented by $^{*}p<0.05$ and $^{**}p<0.01$, respectively.
doi:10.1371/journal.pone.0094115.g002

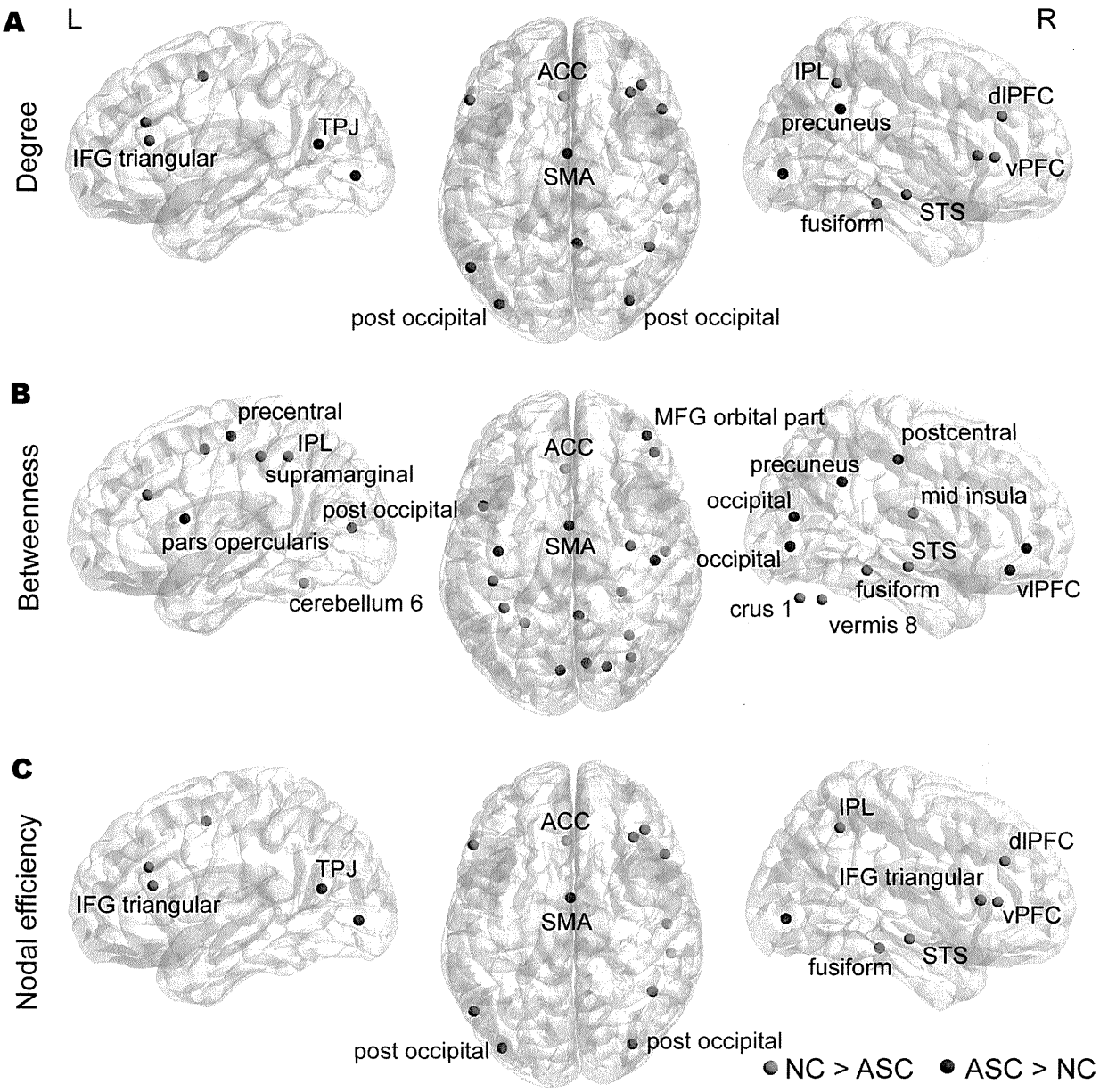

Figure 3. Altered local metrics of degree; betweenness; and nodal efficiency. Alterations in each of local metrics, including degree (A), betweenness (B), and nodal efficiency (C), were observed. The red sphere indicates NC>ASC, while the blue sphere denotes ASC>NC. Of note, in this study, the right inferior temporal [52, −15, −13] was regarded as the right superior temporal sulcus (STS), because this node was anatomically located on the STS rather than the inferior temporal. See Table S3 for other nodes re-labeled in this study. The distributions of nodes showing altered local metrics were visualized with the Brain Net Viewer (http://www.nitrc.org/projects/bnv/).
doi:10.1371/journal.pone.0094115.g003

that network organization in the ASC brain shifts toward randomization compared to that in the NC brain [39,68]. In analyses of the local metrics, increases were observed primarily in the occipital (OC) and sensorimotor (SE) networks, while reductions were found in the fronto-parietal (FP) and cingulo-opercular (CO) networks in participants with ASC, compared with NCs. We also observed that, while both groups shared some nodes as common hubs, each group had several group-specific hubs, indicating changes in hub organization in ASC. Indeed, such changes were confirmed by analyses of all the three hub disruption indices. Subsequent partial correlation analyses demonstrated significant associations between the total AQ score and two local metrics (degree k and nodal efficiency e) of the left ACC. These findings indicate that the influence of nodes is significantly altered in the ASC brain and such alteration is particularly characterized by changes of "hubness" in several nodes critical for social and non-social cognition, both of which are profoundly impaired in people with ASC.

Table 2. The number of affected nodes (NC>ASC or ASC>NC) and non-affected nodes.

Type†	Affected nodes††		Non-affected nodes††
	NC>ASC	ASC>NC	
FP (21)	4 (19%)	1 (4.8%)	16 (76.2%)
CO (32)	4 (12.5%)	2 (6.3%)	26 (81.3%)
DEF (34)	2 (5.9%)	2 (5.9%)	30 (88.2%)
OC (22)	0 (0%)	5 (22.7%)	17 (77.3%)
SE (33)	2 (6.1%)	3 (9.1%)	28 (84.9%)
CER (18)	3 (16.7%)	0 (0%)	15 (83.3%)

†The numbers in parentheses indicate the number of nodes in each sub-network.
††The percentages in parentheses indicate the proportion of affected (or non-affected) nodes to the total number of nodes in each sub-network.
FP: fronto-parietal, CO: cingulo-opercular, DEF: default-mode, OC: occipital, SE: sensorimotor, CER: cerebellar.
doi:10.1371/journal.pone.0094115.t002

1. Altered Global Network Organization in ASC

A recent study demonstrated that adolescents with ASC exhibited enhanced global integration (decreased characteristic path length L) and disrupted local segregation (decreased clustering coefficient C) compared with neurotypical counterparts [39]. Although almost all of the examined global metrics in adults with ASC were consistent with those previously reported for adolescents with ASC [39], only normalized clustering coefficient γ showed a discrepancy between adolescents and adults with ASC; while adolescents with ASC showed a significant reduction in this metric, it was comparable in adults (see Figure S2C). This discrepancy may reflect a normalization process from puberty to adulthood in ASC, which has been often observed for other structural measures (e.g., fractional anisotropy [69]). To investigate this possibility, future investigations need to directly compare data from the two developmental stages obtained in the same experimental setting.

In addition to C and L, we examined the assortativity r of the network; r quantifies whether nodes preferentially connect to nodes with similar degrees. A network is assortative if $r>0$ and random if $r=0$ [70]. Compared with neurotypical brain networks, autistic brain networks were less assortative but not disassortative (i.e., $r>0$), providing further evidence of increased randomness in the network [39,68]. Given that functional connectivity used for constructing a network in this study could be considered as an indirect measure of anatomical connectivity, disruptions of anatomical brain network may possibly induce atypical organization of functional brain network in ASC. Indeed, several diffusion tensor imaging (DTI) studies have demonstrated that people with ASC show alterations in local anatomical pathways, such as the inferior longitudinal fasciculus and uncinate fasciculus [71]. Although no DTI data are available to confirm the link between anatomical and functional brain networks of ASC on a topological space, our findings on global metrics indicate that the tendency of increased randomness in functional network may reflect disrupted anatomical network organization in the ASC brain.

2. Alterations of Local Metrics in ASC

At the nodal level, increased local metrics of degree k, betweenness b, and nodal efficiency e, were primarily observed within the occipital (OC) and sensorimotor (SE) networks, while reductions were mainly observed in the fronto-parietal (FP) and cingulo-opercular (CO) networks in ASC. The FP and CO networks are thought to be critical for adaptive control and stable set maintenance, respectively [72,73]. Previous fMRI studies have revealed that individuals with ASC often show abnormal activation or atypical connections within the FP network during cognitive control and executive function tasks [74–76]. Furthermore, a recent fMRI study using pattern classification analysis demonstrated that the degree of nodes within the CO network contributed to improved classification of the diagnostic status between neurotypical and ASC individuals [36], indicating significant functional alterations in the CO network that may be characteristic to ASC.

Within the CO network, the left ACC exhibited significant reductions in all three local metrics, together with significant negative correlations between the AQ score and k and e. Previous studies on ASC have reported reduced brain activation in the ACC during a number of different cognitive tasks [77,78], as well as during rest [3]. This region is thought to be important for various cognitive and affective functions, including emotional processing [79], conflict monitoring [80], and the learning and selection of high-level behavioral plans [81]. Together with these previous findings, our results suggest that malfunction of the ACC may contribute to impairments in these diverse cognitive and affective functions in ASC.

Notably, significant increases in all three local metrics were observed in the SMA, which is implicated in multiple roles mainly related to movement (e.g., memory-guided movement sequencing) [82]. Although motor dysfunctions may not be always included in the core clinical symptoms of ASC [83,84], clinical observations related to abnormal motions are frequently reported in people with ASC, raising the possibility that people with ASC may have motor network dysfunctions. Indeed, several neuroimaging studies have reported that people with ASC exhibit altered brain activity or functional connectivity in the SMA during motor tasks [85–88]. For example, Takarae et al. demonstrated reduced brain activation in the portion of the SMA (supplementary eye field) during visually guided saccades [87]. Taken together, increased local metrics in this node may reflect such atypical brain activation or connectivity that underlies motor dysfunctions in ASC.

3. Loss of Hubs in the Social-Communication Network of Autism

Several studies have identified functional hubs using several topological metrics (e.g., degree, betweenness, and nodal efficiency) [13–17,89]. In this study, most of the previously reported hubs were replicated using at least one of the three local metrics (e.g., the right precuneus, anterior insula, left inferior parietal lobule) (see Figures S4, S5, and S6), except in a few nodes (e.g., the SMA).

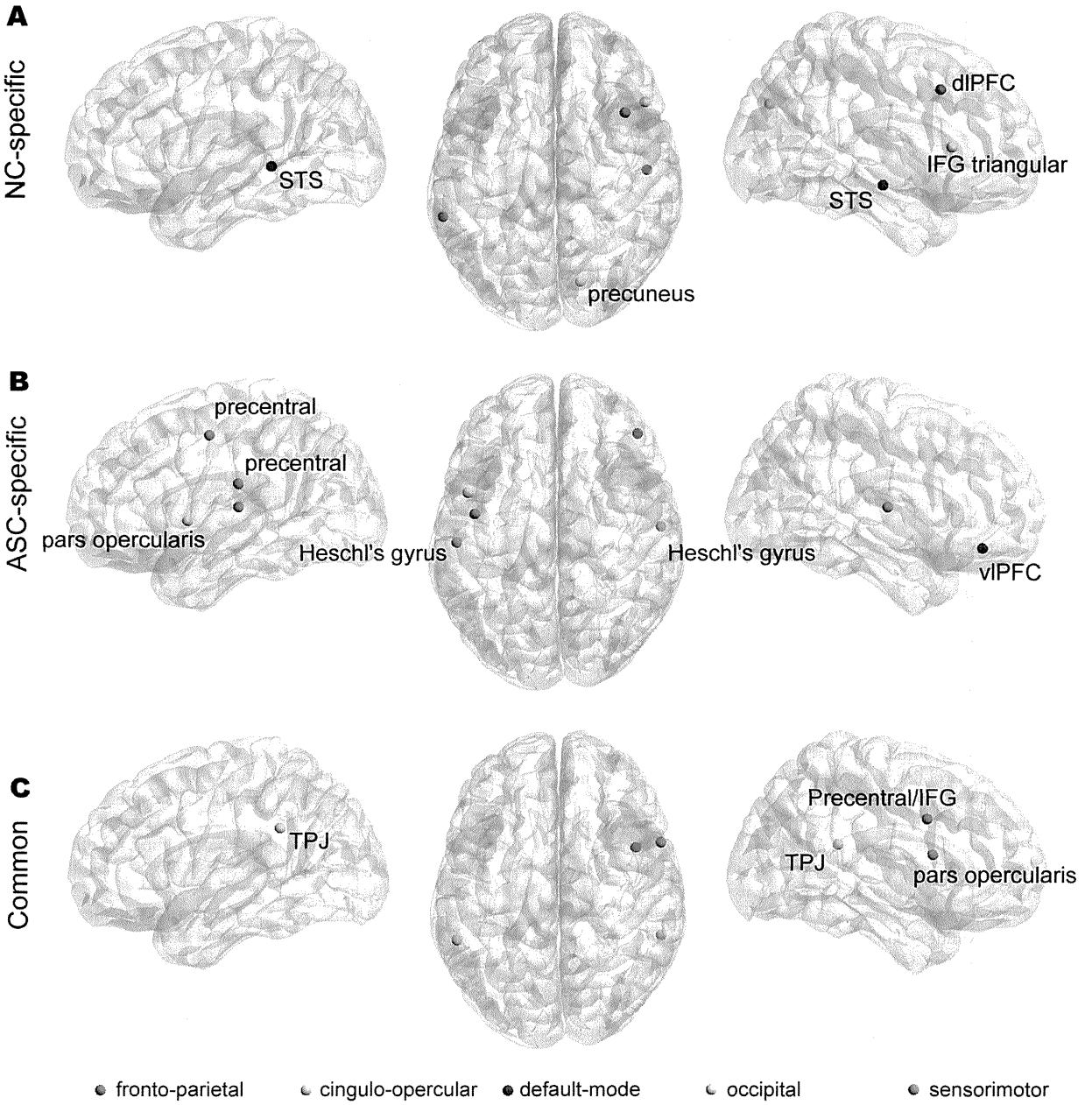

Figure 4. Hub nodes identified using the bootstrap method. The first row shows five NC-specific hubs (A), the second row shows six ASC-specific hubs (B), and the last row shows four common hubs (C). Hub distribution was visualized with the BrainNet Viewer (http://www.nitrc.org/projects/bnv/). Correspondences between colors and networks are as follows: fronto-parietal = red; cingulo-opercular = green; default mode = blue; occipital = cyan; sensorimotor = magenta.
doi:10.1371/journal.pone.0094115.g004

Notably, four nodes (the right precentral/IFG, bilateral TPJ, and right IFG pars opercularis) were identified as common hubs, while five nodes (the bilateral STS, right dlPFC, and right precuneus) and six nodes (the right vlPFC, left IFG pars opercularis, bilateral precentral gyri, and bilateral Heschl's gyri) were identified as NC-specific and ASC-specific hubs, respectively.

Several lines of evidence suggest that dysfunction of the mirror neuron system (MNS) may account for a socio-communicative deficit, which is one of the core clinical symptoms in people with ASC [90,91]. This system involves the right IFG and STS [92] and is thought to represent the actions of others and intentions associated with those actions. The right IFG is one of the central nodes in the MNS and is involved in directing social interaction [93]. Several studies have reported morphological and functional abnormalities in ASC, including reduced gray matter volume [94,95] and reduced neural activity during social tasks [96]. In this study, the right IFG pars opercularis was determined to be a hub in both NC and ASC networks, whereas functional connections

Table 3. A list of hub nodes identified using the Bootstrapping method.

Label	Coordinate	Type	Hub score†	
			NC	ASC
NC-specific hubs				
dlPFC R	40, 17, 40	FP	**2.48**	1.61
IFG triangular R	51, 23, 8	CO	**2.95**	1.10
STS R	52, −15, −13	DEF	**2.15**	0.38
STS L	−61, −41, −2	DEF	**2.43**	1.19
Precuneus R	15, −77, 32	OC	**2.31**	1.08
ASC-specific hubs				
IFG pars opercularis L	−48, 6, 1	CO	1.86	**2.85**
vlPFC R	46, 39, −15	DEF	0.45	**2.76**
Precentral L	−44, −6, 49	SE	1.75	**2.82**
Precentral L	−54, −22, 22	SE	1.12	**2.66**
Heschl's gyrus R	59, −13, 8	SE	1.93	**2.69**
Heschl's gyrus L	−54, −22, 9	SE	1.16	**2.32**
Common hubs				
Precentral/IFG R	44, 8, 34	FP	**2.71**	**2.28**
TPJ R	58, −41, 20	CO	**2.42**	**2.12**
TPJ L	−55, −44, 30	CO	**2.35**	**2.55**
IFG pars opercularis R	58, 11, 14	SE	**2.88**	**2.99**

†Hub score was calculated as the summation of frequencies across all the three local metrics, and then a node with high hub score (≥2.1) was considered as a hub in this study.
FP: fronto-parietal, CO: cingulo-opercular, DEF: default-mode, OC: occipital, SE: sensorimotor.
doi:10.1371/journal.pone.0094115.t003

between this node and several nodes (e.g., the right anterior insula and left ACC) were decreased for ASC, as indicated by functional connectivity analysis (see Figure S7 and Table S4). Although no over-connections with this node were observed in this study, a recent fMRI study reported over-connectivity between this region and others, involving the bilateral OFC, right putamen, and accumbens [97]. Therefore, the observation that the right IFG retained hubness in ASC in the presence of several reduced functional connections may be suggestive of the existence of complementary over-connection with other nodes, possibly at sub-threshold levels.

The right STS was the only NC-specific hub and showed significant reductions across all three local metrics in the ASC group. This region has been demonstrated to play key roles in several social perceptions, such as the perception of eye gaze and biological motion [93]. This node, particularly the posterior part of the STS, has been proposed as one of the core regions responsible for social perceptual impairments in ASC [98]. Consistent with this view, a number of previous studies on ASC have reported abnormalities in this area, such as cortical thinning [99], volumetric reductions [100], under-connectivity between this node and other regions (e.g., amygdala) [101], and atypical functional segregation of the posterior STS [102]. In this study, no under-connections with this node were observed, and no significant associations between any of the local metrics of this node and the AQ score were found. However, in support of the view of mirror neuron dysfunction, the loss of hubness in the right STS together with significant reductions in all three local metrics may underlie socio-cognitive deficits in ASC.

It is noteworthy that six ASC-specific hubs, including the right vlPFC, bilateral precentral gyri, bilateral primary auditory cortices (Heschl's gyri), and left pars opercularis, were identified in this study. As shown in some behavioral studies [103,104], people with ASC have difficulties in the inhibition of inappropriate behaviors. A recent fMRI study demonstrated that, while neurotypical adults showed no recruitment of the right vlPFC, adults with ASC showed atypical hyper-recruitment of the right vlPFC during inhibition control to socially relevant stimuli [74]. Therefore, the hubness in this node may reflect the atypical functional circuitry in the ASC brain. In addition to deficits in social and communicative functions, people with ASC often show impairments in sensory processing. In particular, auditory hypersensitivity is one of the common sensory impairments in ASC, and several behavioral studies have reported deficits in auditory filtering [105–107]. A recent magnetoencephalographic study reported that children with ASC showed longer M50 and M100 peak latencies compared to neurotypical children and that those long latencies were negatively correlated with the severity of auditory hypersensitivity [108]. Furthermore, Hyde et al. recently reported increased cortical thickness in the bilateral primary auditory cortices in the ASC brain [109]. Although no clinical and behavioral data regarding altered sensations are available in this study, our findings on the primary auditory cortex may reflect abnormalities in auditory processing in ASC.

The altered hub organization revealed in this study was also summarized as a disruption of hub rank order. Even though declines in the hub disruption indices were moderate compared to those in comatose patients (ASC: $\kappa_D = -0.22$; comatose [65]: $\kappa_D = -0.82$), the ASC group still showed clear significant reductions of the indices in all three local metrics such that some hubs in the normal brain network (e.g., the right STS) were non-hubs in the ASC brain. Although no significant correlations

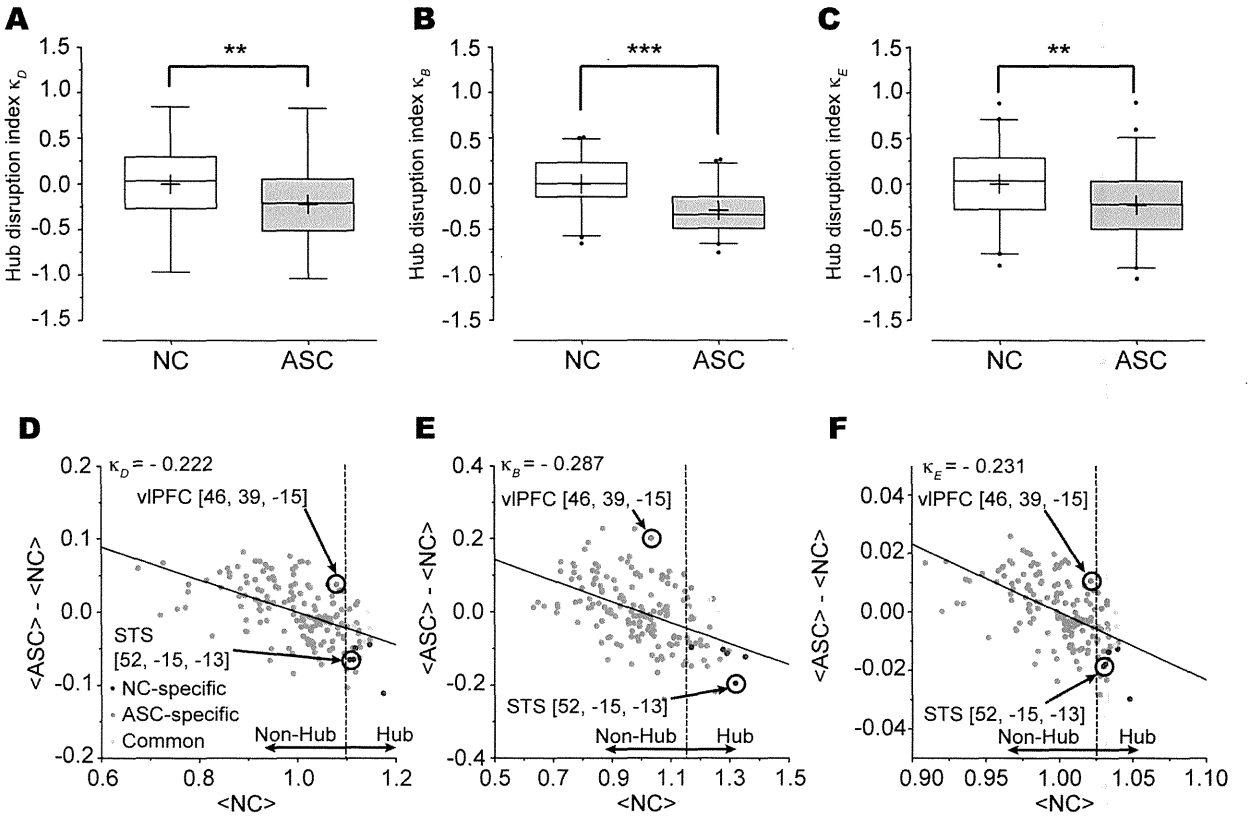

Figure 5. Hub disruption index for each of the three normalized local network metrics of degree; betweenness; and nodal efficiency. The ASC group (gray) exhibited significant reductions in all the three hub disruption indices (κ_D: $p = 0.007$; κ_B: $p < 0.001$; κ_E: $p = 0.006$) (A, B, and C). For illustrative purposes, each of the local metrics was averaged, and then the hub disruption index was calculated at the group level (D, E, and F). Each of hub disruption indices showed significantly negative values in the ASC group, indicating the disruption of hub organization. The colors represent the following groups: NC-specific hub: blue, ASC-specific hub: red, common hub: green. Of note, nodes with high hub scores (≥2.1) were considered as hubs in this study. Significance levels are denoted by $^{**}p<0.01$ and $^{***}p<0.001$, respectively.
doi:10.1371/journal.pone.0094115.g005

between hub disruption indices and the AQ score were found in this study, future studies are needed to address the possibility that a range of dysfunctions involving socio-communicative deficits, dyspraxia, auditory hypersensitivity in ASC might arise from changes in the order of node importance in functional brain network.

Consistent with our results regarding hubness and hub disruption indices, functional connectivity analyses revealed weakened functional connections between nodes in the large-scale system composed of the MNS, limbic system, and insula (see Text S2 and Table S4). The insula is anatomically connected with brain regions within the MNS and limbic system, and this system as a whole has been proposed to facilitate the understanding of other people's emotions through action representation [110]. Therefore, our results suggest that poor communication between the MNS and limbic system through the anterior insula may contribute to social cognitive and affective dysfunctions in ASC. In addition, reduced functional connections were also found in the motor network involving the precentral gyrus, cerebellum, and putamen, which may potentially explain ASC-associated motor deficits [86,87,111,112]. Taken together, our findings on functional connectivity are in line with the view that ASC is characterized by an array of dysfunctions including the hallmark deficits in social and communicative functions.

It would also be important in future studies to link the observed pattern of altered functional networks with molecular and genetic findings to advance our understanding of the pathological mechanisms of ASC. Molecular basis of ASC is associated with many of the synaptic cell-adhesion molecules, including neurexins, neuroligins, and cadherins [113–116], all of which play important roles in determining aspects of neural connections including synaptic formation and axonal guidance. Altered expressions of genes encoding these molecules might lead to the development of altered functional network for ASC that displays the characteristics of brain connectivity revealed by the present study.

4. Limitations

There are several limitations in the present study. Firstly, functional brain networks were constructed using the 160 functional ROIs defined by Dosenbach et al. [55], while previous studies have often employed anatomical ROIs (e.g., an automated anatomical labeling atlas). There is evidence that differences in node definition can affect the resulting topological architecture [117–119]. In addition, the set of nodes used in this study does not include certain limbic regions (e.g., amygdala) that are important in clinical populations. However, the set of nodes used here exhibited better reliability than the anatomical scheme for calculating the network topology [120], and the same node

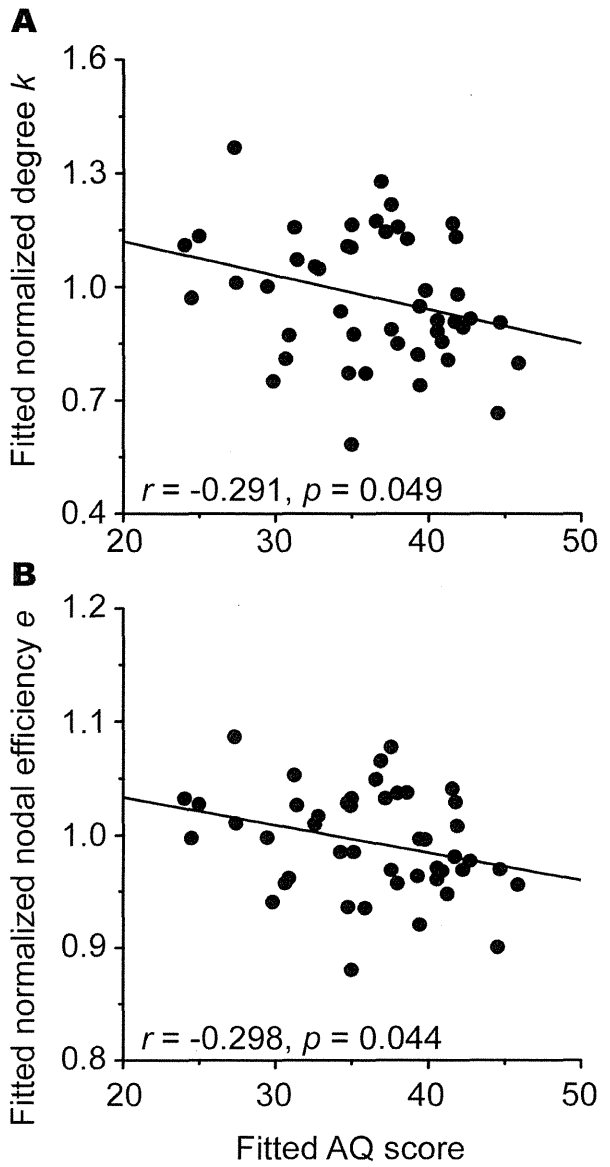

Figure 6. Scatter plots of degree and nodal efficiency of the left ACC against AQ score. Partial correlation analyses revealed that there were the significant negative correlations between the AQ score and two of the local metrics of the ACC (*k*: $r = -0.291$, $p = 0.049$; *e*: $r = -0.298$, $p = 0.044$).
doi:10.1371/journal.pone.0094115.g006

definition was used in several network studies [17,36]. Moreover, the fact that our findings on global metrics were consistent with the results of a previous study of adolescents with ASC [39] further supports the validity of our analyses.

Secondly, the frequency band of the analyzed resting-state brain activity was restricted to the low frequency range due to limitations in the temporal resolution of fMRI, and the relatively sluggish nature of the hemodynamic response. In this study, we applied a band-pass filter (0.009–0.08 Hz) to remove artifacts, because low-frequency spontaneous fluctuations of rs-fMRI signals within this range are thought to reflect neurophysiological processes of the human brain [121,122]. On the other hand, abnormal brain activities in different frequency bands have been reported in people with ASC based on electroencephalography (EEG) data [31,34]. In future studies, it will be important to examine the topological properties of the functional brain network in individuals with ASC using both electrophysiologically and hemodynamically derived signals.

Thirdly, some demographic information (IQ and handedness) was missing in this study. To validate our main findings, we repeated the second-level analyses of all the 8 global metrics on 39 NCs and 45 participants with ASC, and confirmed that, in spite of reduced statistical power, statistical conclusions were preserved for all the 8 measures (see Figure S8). Although gender differences might be one of the confounding factors, the small number of female participants ($n = 7$ in each group) did not allow us to draw statistically rigorous conclusions regarding possible gender effects on the network measures. Further investigations will be needed to examine the gender effects on the topological metrics.

Lastly, we examined the topological properties of the resting-state functional brain network, while state-dependent topological changes have been reported in ASC [36] and schizophrenia [25]. Hence, exploring network topologies during tasks would also be important for developing a complete understanding of the ASC brain.

Conclusions

Our findings revealed significant alterations in global network topologies, as well as changes in the order of node importance and the loss of hubness associated with social and non-social functions in ASC. Consistent with previous findings [39,68], our results suggest that the autistic brain network is likely to be randomized compared to the neurotypical one. At the nodal level, the left ACC and right STS might contribute to socio-communicative deficiencies in ASC. Advances in the modeling of functional brain networks have provided powerful methodological frameworks to reveal the neuronal alterations underlying atypical behaviors in ASC.

Supporting Information

Figure S1 Effects of the scrubbing method. Using the frame-wise displacement metric with a 0.5 mm threshold, the motion-contaminated volumes were detected in 16 NCs and 12 participants with ASC, respectively. The first row shows the effects of the scrubbing method for the average of 16 NCs (A to C), and the second row shows the effects for the average of 12 participants with ASC (D to F). The first column shows the correlation matrices for both groups, calculated without applying the scrubbing method (for simplicity, we will refer these as "standard") (A and D); the second column shows the correlation matrices calculated with the scrubbing method (henceforth, we will refer these as "scrubbed") (B and E); the last column shows the difference between the standard and scrubbed matrices (C and F). We observed slightly decreased correlation values in the short-range, and increased correlation values in the long-range after adopting the scrubbing method. For example, the correlation between the right vPFC [34,32,7] and right vlPFC [39,42,16] was decreased after the removal of motion-contaminated volumes ($D = 14.25$ mm; $\Delta r = -0.01$), while the correlation between the right vmPFC [6,64,3] and left post occipital [−37, −83, −2] was increased after scrubbing ($D = 153.24$ mm; $\Delta r = 0.016$). FP: fronto-parietal, CO: cingulo-opercular, DEF: default mode, OC: occipital, SE: sensorimotor, CER: cerebellar, *D*: the Euclidean distance between node A and node B.
(TIF)

Figure S2 Global metrics of global efficiency, E_{glob}, local efficiency, E_{loc}, normalized clustering coefficient, γ, and normalized characteristic path length, λ, as functions of the sparsity threshold. The error bar indicates the standard error of the mean (SEM). Compared with the NC group (blue line), the ASC group (red line) showed significantly higher E_{glob} and lower E_{loc} and λ ($p<0.05$, FDR corrected) over the range of sparsity thresholds (A, B, and D), whereas γ was comparable between the groups (C).
(TIF)

Figure S3 Between-group differences in the AUC values of global efficiency, E_{glob}, local efficiency, E_{loc}, normalized clustering coefficient, γ, and normalized characteristic path length, λ. In the AUC analyses, participants with ASC (black) exhibited significantly higher E_{glob} ($p = 0.02$) (A), and significantly lower E_{loc} ($p = 0.011$) (B) and λ ($p = 0.001$) (D), while γ was comparable between the groups (D). Significance levels are represented by $*p<0.05$ and $**p<0.01$, respectively.
(TIF)

Figure S4 Functional hubs were identified using degree and bootstrapping method. The first row shows ten "NC-specific" hubs, involving the bilateral anterior insula, left STS, the bilateral dlPFC, and right IFG triangular; the second row shows six "ASC-specific" hubs, including the right vlPFC, left precentral gyrus, and left Heschl's gyrus; and the last row shows five "common" hubs (the right dlPFC, left IPL, TPJ, and left IFG pars opercularis). Correspondences between colors and networks are as follows: fronto-parietal = red; cingulo-opercular = green; default mode = blue; sensorimotor = magenta. Hubs were visualized with the BrainNet Viewer (http://www.nitrc.org/projects/bnv/).
(TIF)

Figure S5 Functional hubs were identified using betweenness and bootstrapping method. The first row shows eight "NC-specific" hubs, involving the bilateral STS, left precuneus, the bilateral crus 1, and right IFG triangular; the second row shows 11 "ASC-specific" hubs, including the SMA, the right vlPFC, left TPJ, and right Heschl's gyrus; and the last row shows seven "common" hub, encompassing the bilateral precuneus, the right TPJ, the right IFG pars opercularis, and left precentral. Correspondences between colors and networks are as follows: fronto-parietal = red; cingulo-opercular = green; default mode = blue; occipital = cyan; sensorimotor = magenta; cerebellar = yellow. Hubs were visualized with the BrainNet Viewer (http://www.nitrc.org/projects/bnv/).
(TIF)

Figure S6 Functional hubs were identified using nodal efficiency and bootstrapping method. The first row shows nine "NC-specific" hubs, involving the bilateral anterior insula, the left STS, the left ACC, the right dlPFC, and right IFG triangular; the second row shows five "ASC-specific" hubs, including the right vlPFC, left precentral, left angular gyrus, and left Heschl's gyrus; and the last row shows seven "common" hub, encompassing the bilateral IFG pars opercularis, and right dlPFC. Correspondences between colors and networks are as follows: fronto-parietal = red; cingulo-opercular = green; default mode = blue; sensorimotor = magenta. Hubs were visualized with the BrainNet Viewer (http://www.nitrc.org/projects/bnv/).
(TIF)

Figure S7 Reduced functional connectivity in participants with ASC identified using the network-based statistic approach. The reduced connections were found mainly within the cingulo-opercular network rather than within the default mode network. Correspondences between colors and networks are as follows: fronto-parietal = red; cingulo-opercular = green; default mode = blue; sensorimotor = magenta; cerebellar = yellow. These reduced connections were visualized with the BrainNet Viewer (http://www.nitrc.org/projects/bnv/).
(TIF)

Figure S8 Between group differences in the AUC values of all the global measures performed on 39 NCs and 45 participants with ASC. The second-level analyses were re-conducted on 39 NCs and 45 ASC participants to ensure that between-group differences were not due to differences in handedness. Statistical conclusions were preserved for all the global metrics (clustering coefficient: $p = 0.048$, characteristic path length: $p = 0.012$; assortativity: $p = 0.032$; small-worldness: $p = 0.083$; global efficiency: $p = 0.018$; local efficiency: $p = 0.044$; normalized clustering coefficient: $p = 0.170$; normalized characteristic path length: $p = 0.013$). Significance levels are represented by $*p<0.05$ and $**p<0.01$, respectively.
(TIF)

Table S1 Brief description of network metrics used in this study.
(DOC)

Table S2 Altered local network metrics (degree *k*, betweenness *b*, and nodal efficiency *e*) in the ASC group compared to the NC group.
(DOC)

Table S3 A list of re-labeled nodes in this study.
(DOC)

Table S4 Reduced functional connectivity in participants with ASC compared to NCs.
(DOC)

Text S1 The details of scrubbing method used in this study.
(DOC)

Text S2 Functional connectivity analysis.
(DOC)

Author Contributions

Conceived and designed the experiments: RH. Performed the experiments: TY HW MN RH. Analyzed the data: TI RH. Contributed reagents/materials/analysis tools: TI RH. Wrote the paper: TI RH. Supervision: NK KT DJ SS.

References

1. American Psychiatric Association (2013) Diagnostic and statistical manual of mental disorders: DSM-5. Arlington, VA: American Psychiatric Publishing.
2. Uddin LQ, Supekar K, Menon V (2013) Reconceptualizing functional brain connectivity in autism from a developmental perspective. Front Hum Neurosci 7: 458.
3. Assaf M, Jagannathan K, Calhoun VD, Miller L, Stevens MC, et al. (2010) Abnormal functional connectivity of default mode sub-networks in autism spectrum disorder patients. Neuroimage 53: 247–256.
4. von dem Hagen EA, Stoyanova RS, Baron-Cohen S, Calder AJ (2013) Reduced functional connectivity within and between 'social' resting state networks in autism spectrum conditions. Soc Cogn Affect Neurosci 8: 694–701.
5. Di Martino A, Yan CG, Li Q, Denio E, Castellanos FX, et al. (2013) The autism brain imaging data exchange: towards a large-scale evaluation of the intrinsic brain architecture in autism. Mol Psychiatry.
6. Supekar K, Uddin LQ, Khouzam A, Phillips J, Gaillard WD, et al. (2013) Brain hyperconnectivity in children with autism and its links to social deficits. Cell Rep 5: 738–747.

7. Muller RA (2007) The study of autism as a distributed disorder. Ment Retard Dev Disabil Res Rev 13: 85–95.
8. Bullmore ET, Bassett DS (2011) Brain graphs: graphical models of the human brain connectome. Annu Rev Clin Psychol 7: 113–140.
9. Bullmore E, Sporns O (2009) Complex brain networks: graph theoretical analysis of structural and functional systems. Nat Rev Neurosci 10: 186–198.
10. Watts DJ, Strogatz SH (1998) Collective dynamics of 'small-world' networks. Nature 393: 440–442.
11. Achard S, Salvador R, Whitcher B, Suckling J, Bullmore E (2006) A resilient, low-frequency, small-world human brain functional network with highly connected association cortical hubs. J Neurosci 26: 63–72.
12. Bassett DS, Bullmore E (2006) Small-world brain networks. Neuroscientist 12: 512–523.
13. Tian L, Wang J, Yan C, He Y (2011) Hemisphere- and gender-related differences in small-world brain networks: a resting-state functional MRI study. Neuroimage 54: 191–202.
14. Fransson P, Aden U, Blennow M, Lagercrantz H (2011) The functional architecture of the infant brain as revealed by resting-state fMRI. Cereb Cortex 21: 145–154.
15. He Y, Wang J, Wang L, Chen ZJ, Yan C, et al. (2009) Uncovering intrinsic modular organization of spontaneous brain activity in humans. PLoS One 4: e5226.
16. Buckner RL, Sepulcre J, Talukdar T, Krienen FM, Liu H, et al. (2009) Cortical hubs revealed by intrinsic functional connectivity: mapping, assessment of stability, and relation to Alzheimer's disease. J Neurosci 29: 1860–1873.
17. Hwang K, Hallquist MN, Luna B (2013) The development of hub architecture in the human functional brain network. Cereb Cortex 23: 2380–2393.
18. Fair DA, Cohen AL, Power JD, Dosenbach NU, Church JA, et al. (2009) Functional brain networks develop from a "local to distributed" organization. PLoS Comput Biol 5: e1000381.
19. Fan Y, Shi F, Smith JK, Lin W, Gilmore JH, et al. (2011) Brain anatomical networks in early human brain development. Neuroimage 54: 1862–1871.
20. Meunier D, Achard S, Morcom A, Bullmore E (2009) Age-related changes in modular organization of human brain functional networks. Neuroimage 44: 715–723.
21. Menon V (2013) Developmental pathways to functional brain networks: emerging principles. Trends Cogn Sci 17: 627–640.
22. Kleinhans NM, Pauley G, Richards T, Neuhaus E, Martin N, et al. (2012) Age-related abnormalities in white matter microstructure in autism spectrum disorders. Brain Res 1479: 1–16.
23. Alexander-Bloch AF, Gogtay N, Meunier D, Birn R, Clasen L, et al. (2010) Disrupted modularity and local connectivity of brain functional networks in childhood-onset schizophrenia. Front Syst Neurosci 4: 147.
24. Bassett DS, Nelson BG, Mueller BA, Camchong J, Lim KO (2012) Altered resting state complexity in schizophrenia. Neuroimage 59: 2196–2207.
25. Fornito A, Zalesky A, Pantelis C, Bullmore ET (2012) Schizophrenia, neuroimaging and connectomics. Neuroimage 62: 2296–2314.
26. Liu Y, Liang M, Zhou Y, He Y, Hao Y, et al. (2008) Disrupted small-world networks in schizophrenia. Brain 131: 945–961.
27. Lynall ME, Bassett DS, Kerwin R, McKenna PJ, Kitzbichler M, et al. (2010) Functional connectivity and brain networks in schizophrenia. J Neurosci 30: 9477–9487.
28. Zhang J, Wang J, Wu Q, Kuang W, Huang X, et al. (2011) Disrupted brain connectivity networks in drug-naive, first-episode major depressive disorder. Biol Psychiatry 70: 334–342.
29. Bruno J, Hosseini SM, Kesler S (2012) Altered resting state functional brain network topology in chemotherapy-treated breast cancer survivors. Neurobiol Dis 48: 329–338.
30. Sanz-Arigita EJ, Schoonheim MM, Damoiseaux JS, Rombouts SA, Maris E, et al. (2010) Loss of 'small-world' networks in Alzheimer's disease: graph analysis of FMRI resting-state functional connectivity. PLoS One 5: e13788.
31. Barttfeld P, Wicker B, Cukier S, Navarta S, Lew S, et al. (2011) A big-world network in ASD: dynamical connectivity analysis reflects a deficit in long-range connections and an excess of short-range connections. Neuropsychologia 49: 254–263.
32. Tsiaras V, Simos PG, Rezaie R, Sheth BR, Garyfallidis E, et al. (2011) Extracting biomarkers of autism from MEG resting-state functional connectivity networks. Comput Biol Med 41: 1166–1177.
33. Li H, Xue Z, Ellmore TM, Frye RE, Wong ST (2012) Network-based analysis reveals stronger local diffusion-based connectivity and different correlations with oral language skills in brains of children with high functioning autism spectrum disorders. Hum Brain Mapp.
34. Peters JM, Taquet M, Vega C, Jeste SS, Fernandez IS, et al. (2013) Brain functional networks in syndromic and non-syndromic autism: a graph theoretical study of EEG connectivity. BMC Med 11: 54.
35. Jakab A, Emri M, Spisak T, Szeman-Nagy A, Beres M, et al. (2013) Autistic traits in neurotypical adults: correlates of graph theoretical functional network topology and white matter anisotropy patterns. PLoS One 8: e60982.
36. Barttfeld P, Wicker B, Cukier S, Navarta S, Lew S, et al. (2012) State-dependent changes of connectivity patterns and functional brain network topology in autism spectrum disorder. Neuropsychologia 50: 3653–3662.
37. Redcay E, Moran JM, Mavros PL, Tager-Flusberg H, Gabrieli JD, et al. (2013) Intrinsic functional network organization in high-functioning adolescents with autism spectrum disorder. Front Hum Neurosci 7: 573.
38. Di Martino A, Zuo XN, Kelly C, Grzadzinski R, Mennes M, et al. (2013) Shared and distinct intrinsic functional network centrality in autism and attention-deficit/hyperactivity disorder. Biol Psychiatry 74: 623–632.
39. Rudie JD, Brown JA, Beck-Pancer D, Hernandez LM, Dennis EL, et al. (2012) Altered functional and structural brain network organization in autism. Neuroimage Clin 2: 79–94.
40. Hua X, Thompson PM, Leow AD, Madsen SK, Caplan R, et al. (2013) Brain growth rate abnormalities visualized in adolescents with autism. Hum Brain Mapp 34: 425–436.
41. Amaral DG, Schumann CM, Nordahl CW (2008) Neuroanatomy of autism. Trends Neurosci 31: 137–145.
42. Courchesne E, Campbell K, Solso S (2011) Brain growth across the life span in autism: age-specific changes in anatomical pathology. Brain Res 1380: 138–145.
43. Langen M, Schnack HG, Nederveen H, Bos D, Lahuis BE, et al. (2009) Changes in the developmental trajectories of striatum in autism. Biol Psychiatry 66: 327–333.
44. Williams DL, Cherkassky VL, Mason RA, Keller TA, Minshew NJ, et al. (2013) Brain function differences in language processing in children and adults with autism. Autism Res 6: 288–302.
45. Dickstein DP, Pescosolido MF, Reidy BL, Galvan T, Kim KL, et al. (2013) Developmental meta-analysis of the functional neural correlates of autism spectrum disorders. J Am Acad Child Adolesc Psychiatry 52: 279–289 e216.
46. Baron-Cohen S, Wheelwright S, Skinner R, Martin J, Clubley E (2001) The autism-spectrum quotient (AQ): evidence from Asperger syndrome/high-functioning autism, males and females, scientists and mathematicians. J Autism Dev Disord 31: 5–17.
47. Matsuoka K (2006) Estimation of premorbid IQ in individuals with Alzheimer's disease using Japanese ideographic script (Kanji) compound words: Japanese version of National Adult Reading Test. Psychiatry Clin Neurosci 60: 332–339.
48. Nelson HE (1982) National Adult Reading Test (NART): For the Assessment of Premorbid Intelligence in Patients with Dementia: Test Manual. NFER-Nelson, Windsor, UK.
49. Nakano M, Matsuo K, Nakashima M, Matsubara T, Harada K, et al. (2014) Gray matter volume and rapid decision-making in major depressive disorder. Prog Neuropsychopharmacol Biol Psychiatry 48: 51–56.
50. Watanabe T, Yahata N, Abe O, Kuwabara H, Inoue H, et al. (2012) Diminished medial prefrontal activity behind autistic social judgments of incongruent information. PLoS One 7: e39561.
51. Oldfield RC (1971) The assessment and analysis of handedness: The Edinburgh inventory. Neuropsychologia 9: 97–113.
52. Wakabayashi A, Baron-Cohen S, Wheelwright S, Tojo Y (2006) The Autism-Spectrum Quotient (AQ) in Japan: A cross-cultural comparison. J Autism Dev Disord 36: 263–270.
53. Cao H, Plichta MM, Schafer A, Haddad L, Grimm O, et al. (2014) Test-retest reliability of fMRI-based graph theoretical properties during working memory, emotion processing, and resting state. Neuroimage 84: 888–900.
54. Liu Y, Liang M, Zhou Y, He Y, Hao Y, et al. (2008) Disrupted small-world networks in schizophrenia. Brain 131: 945–961.
55. Dosenbach NU, Nardos B, Cohen AL, Fair DA, Power JD, et al. (2010) Prediction of individual brain maturity using fMRI. Science 329: 1358–1361.
56. Behzadi Y, Restom K, Liau J, Liu TT (2007) A component based noise correction method (CompCor) for BOLD and perfusion based fMRI. Neuroimage 37: 90–101.
57. Murphy K, Birn RM, Handwerker DA, Jones TB, Bandettini PA (2009) The impact of global signal regression on resting state correlations: are anti-correlated networks introduced? Neuroimage 44: 893–905.
58. Power JD, Barnes KA, Snyder AZ, Schlaggar BL, Petersen SE (2012) Spurious but systematic correlations in functional connectivity MRI networks arise from subject motion. Neuroimage 59: 2142–2154.
59. Van Dijk KR, Sabuncu MR, Buckner RL (2012) The influence of head motion on intrinsic functional connectivity MRI. Neuroimage 59: 431–438.
60. van Wijk BC, Stam CJ, Daffertshofer A (2010) Comparing brain networks of different size and connectivity density using graph theory. PLoS One 5: e13701.
61. Rubinov M, Sporns O (2010) Complex network measures of brain connectivity: uses and interpretations. Neuroimage 52: 1059–1069.
62. Newman M (2003) The Structure and Function of Complex Networks. SIAM Review 45: 167–256.
63. Achard S, Bullmore E (2007) Efficiency and cost of economical brain functional networks. PLoS Comput Biol 3: e17.
64. Zhang Z, Liao W, Chen H, Mantini D, Ding JR, et al. (2011) Altered functional-structural coupling of large-scale brain networks in idiopathic generalized epilepsy. Brain 134: 2912–2928.
65. Achard S, Delon-Martin C, Vértes PE, Renard F, Schenck M, et al. (2012) Hubs of brain functional networks are radically reorganized in comatose patients. Proceedings of the National Academy of Sciences 109: 20608–20613.
66. Benjamini Y, Hochberg Y (1995) Controlling the False Discovery Rate: A Practical and Powerful Approach to Multiple Testing. Journal of the Royal Statistical Society Series B (Methodological) 57: 289–300.
67. Efron B (1979) Bootstrap Methods: Another Look at the Jackknife. The Annals of Statistics 7: 1–26.

68. Lai MC, Lombardo MV, Chakrabarti B, Sadek SA, Pasco G, et al. (2010) A shift to randomness of brain oscillations in people with autism. Biol Psychiatry 68: 1092–1099.
69. Bakhtiari R, Zurcher NR, Rogier O, Russo B, Hippolyte L, et al. (2012) Differences in white matter reflect atypical developmental trajectory in autism: A Tract-based Spatial Statistics study. Neuroimage Clin 1: 48–56.
70. Newman MEJ (2002) Assortative Mixing in Networks. Physical Review Letters 89: 208701.
71. Aoki Y, Abe O, Nippashi Y, Yamasue H (2013) Comparison of white matter integrity between autism spectrum disorder subjects and typically developing individuals: a meta-analysis of diffusion tensor imaging tractography studies. Mol Autism 4: 25.
72. Dosenbach NU, Fair DA, Miezin FM, Cohen AL, Wenger KK, et al. (2007) Distinct brain networks for adaptive and stable task control in humans. Proc Natl Acad Sci U S A 104: 11073–11078.
73. Dosenbach NU, Visscher KM, Palmer ED, Miezin FM, Wenger KK, et al. (2006) A core system for the implementation of task sets. Neuron 50: 799–812.
74. Duerden EG, Taylor MJ, Soorya LV, Wang T, Fan J, et al. (2013) Neural correlates of inhibition of socially relevant stimuli in adults with autism spectrum disorder. Brain Research 1533: 80–90.
75. Greimel E, Nehrkorn B, Fink GR, Kukolja J, Kohls G, et al. (2012) Neural mechanisms of encoding social and non-social context information in autism spectrum disorder. Neuropsychologia 50: 3440–3449.
76. Just MA, Cherkassky VL, Keller TA, Kana RK, Minshew NJ (2007) Functional and anatomical cortical underconnectivity in autism: evidence from an FMRI study of an executive function task and corpus callosum morphometry. Cereb Cortex 17: 951–961.
77. Kana RK, Keller TA, Minshew NJ, Just MA (2007) Inhibitory control in high-functioning autism: decreased activation and underconnectivity in inhibition networks. Biol Psychiatry 62: 198–206.
78. Solomon M, Ozonoff SJ, Ursu S, Ravizza S, Cummings N, et al. (2009) The neural substrates of cognitive control deficits in autism spectrum disorders. Neuropsychologia 47: 2515–2526.
79. Etkin A, Egner T, Kalisch R (2011) Emotional processing in anterior cingulate and medial prefrontal cortex. Trends Cogn Sci 15: 85–93.
80. Botvinick MM, Cohen JD, Carter CS (2004) Conflict monitoring and anterior cingulate cortex: an update. Trends Cogn Sci 8: 539–546.
81. Holroyd CB, Yeung N (2012) Motivation of extended behaviors by anterior cingulate cortex. Trends Cogn Sci 16: 122–128.
82. Gaymard B, Rivaud S, Pierrot-Deseilligny C (1993) Role of the left and right supplementary motor areas in memory-guided saccade sequences. Ann Neurol 34: 404–406.
83. Dowell LR, Mahone EM, Mostofsky SH (2009) Associations of postural knowledge and basic motor skill with dyspraxia in autism: implication for abnormalities in distributed connectivity and motor learning. Neuropsychology 23: 563–570.
84. Dziuk MA, Gidley Larson JC, Apostu A, Mahone EM, Denckla MB, et al. (2007) Dyspraxia in autism: association with motor, social, and communicative deficits. Dev Med Child Neurol 49: 734–739.
85. Di Martino A, Ross K, Uddin LQ, Sklar AB, Castellanos FX, et al. (2009) Functional brain correlates of social and nonsocial processes in autism spectrum disorders: an activation likelihood estimation meta-analysis. Biol Psychiatry 65: 63–74.
86. Mostofsky SH, Powell SK, Simmonds DJ, Goldberg MC, Caffo B, et al. (2009) Decreased connectivity and cerebellar activity in autism during motor task performance. Brain 132: 2413–2425.
87. Takarae Y, Minshew NJ, Luna B, Sweeney JA (2007) Atypical involvement of frontostriatal systems during sensorimotor control in autism. Psychiatry Res 156: 117–127.
88. Muller RA, Cauich C, Rubio MA, Mizuno A, Courchesne E (2004) Abnormal activity patterns in premotor cortex during sequence learning in autistic patients. Biol Psychiatry 56: 323–332.
89. Power JD, Schlaggar BL, Lessov-Schlaggar CN, Petersen SE (2013) Evidence for hubs in human functional brain networks. Neuron 79: 798–813.
90. Iacoboni M, Dapretto M (2006) The mirror neuron system and the consequences of its dysfunction. Nat Rev Neurosci 7: 942–951.
91. Rizzolatti G, Fabbri-Destro M, Cattaneo L (2009) Mirror neurons and their clinical relevance. Nat Clin Pract Neurol 5: 24–34.
92. Rizzolatti G, Fabbri-Destro M (2008) The mirror system and its role in social cognition. Curr Opin Neurobiol 18: 179–184.
93. Blakemore SJ (2008) The social brain in adolescence. Nat Rev Neurosci 9: 267–277.
94. Kosaka H, Omori M, Munesue T, Ishitobi M, Matsumura Y, et al. (2010) Smaller insula and inferior frontal volumes in young adults with pervasive developmental disorders. Neuroimage 50: 1357–1363.
95. Yamasaki S, Yamasue H, Abe O, Suga M, Yamada H, et al. (2010) Reduced gray matter volume of pars opercularis is associated with impaired social communication in high-functioning autism spectrum disorders. Biol Psychiatry 68: 1141–1147.
96. Kana RK, Libero LE, Hu CP, Deshpande HD, Colburn JS (2012) Functional Brain Networks and White Matter Underlying Theory-of-Mind in Autism. Social Cognitive and Affective Neuroscience.
97. Rudie JD, Shehzad Z, Hernandez LM, Colich NL, Bookheimer SY, et al. (2012) Reduced functional integration and segregation of distributed neural systems underlying social and emotional information processing in autism spectrum disorders. Cereb Cortex 22: 1025–1037.
98. Pelphrey KA, Carter EJ (2008) Brain mechanisms for social perception: lessons from autism and typical development. Ann N Y Acad Sci 1145: 283–299.
99. Hadjikhani N, Joseph RM, Snyder J, Tager-Flusberg H (2006) Anatomical differences in the mirror neuron system and social cognition network in autism. Cereb Cortex 16: 1276–1282.
100. Boddaert N, Chabane N, Gervais H, Good CD, Bourgeois M, et al. (2004) Superior temporal sulcus anatomical abnormalities in childhood autism: a voxel-based morphometry MRI study. Neuroimage 23: 364–369.
101. Abrams DA, Lynch CJ, Cheng KM, Phillips J, Supekar K, et al. (2013) Underconnectivity between voice-selective cortex and reward circuitry in children with autism. Proceedings of the National Academy of Sciences 110: 12060–12065.
102. Shih P, Keehn B, Oram JK, Leyden KM, Keown CL, et al. (2011) Functional differentiation of posterior superior temporal sulcus in autism: a functional connectivity magnetic resonance imaging study. Biol Psychiatry 70: 270–277.
103. Christ SE, Holt DD, White DA, Green L (2007) Inhibitory control in children with autism spectrum disorder. J Autism Dev Disord 37: 1155–1165.
104. Mosconi MW, Kay M, D'Cruz AM, Seidenfeld A, Guter S, et al. (2009) Impaired inhibitory control is associated with higher-order repetitive behaviors in autism spectrum disorders. Psychol Med 39: 1559–1566.
105. Ashburner J, Ziviani J, Rodger S (2008) Sensory processing and classroom emotional, behavioral, and educational outcomes in children with autism spectrum disorder. Am J Occup Ther 62: 564–573.
106. Dunn MA, Gomes H, Gravel J (2008) Mismatch negativity in children with autism and typical development. J Autism Dev Disord 38: 52–71.
107. Lane A, Young R, Baker AZ, Angley M (2010) Sensory Processing Subtypes in Autism: Association with Adaptive Behavior. Journal of Autism and Developmental Disorders 40: 112–122.
108. Matsuzaki J, Kagitani-Shimono K, Goto T, Sanefuji W, Yamamoto T, et al. (2012) Differential responses of primary auditory cortex in autistic spectrum disorder with auditory hypersensitivity. Neuroreport 23: 113–118.
109. Hyde KL, Samson F, Evans AC, Mottron L (2010) Neuroanatomical differences in brain areas implicated in perceptual and other core features of autism revealed by cortical thickness analysis and voxel-based morphometry. Hum Brain Mapp 31: 556–566.
110. Carr L, Iacoboni M, Dubeau MC, Mazziotta JC, Lenzi GL (2003) Neural mechanisms of empathy in humans: a relay from neural systems for imitation to limbic areas. Proc Natl Acad Sci U S A 100: 5497–5502.
111. Allen G, Muller RA, Courchesne E (2004) Cerebellar function in autism: functional magnetic resonance image activation during a simple motor task. Biol Psychiatry 56: 269–278.
112. Nebel MB, Joel SE, Muschelli J, Barber AD, Caffo BS, et al. (2012) Disruption of functional organization within the primary motor cortex in children with autism. Hum Brain Mapp.
113. Arons MH, Thynne CJ, Grabrucker AM, Li D, Schoen M, et al. (2012) Autism-associated mutations in ProSAP2/Shank3 impair synaptic transmission and neurexin-neuroligin-mediated transsynaptic signaling. J Neurosci 32: 14966–14978.
114. Foldy C, Malenka RC, Sudhof TC (2013) Autism-associated neuroligin-3 mutations commonly disrupt tonic endocannabinoid signaling. Neuron 78: 498–509.
115. Redies C, Hertel N, Hubner CA (2012) Cadherins and neuropsychiatric disorders. Brain Res 1470: 130–144.
116. Jamain S, Quach H, Betancur C, Rastam M, Colineaux C, et al. (2003) Mutations of the X-linked genes encoding neuroligins NLGN3 and NLGN4 are associated with autism. Nat Genet 34: 27–29.
117. Hayasaka S, Laurienti PJ (2010) Comparison of characteristics between region- and voxel-based network analyses in resting-state fMRI data. Neuroimage 50: 499–508.
118. Wang J, Wang L, Zang Y, Yang H, Tang H, et al. (2009) Parcellation-dependent small-world brain functional networks: a resting-state fMRI study. Hum Brain Mapp 30: 1511–1523.
119. Zalesky A, Fornito A, Harding IH, Cocchi L, Yucel M, et al. (2010) Whole-brain anatomical networks: does the choice of nodes matter? Neuroimage 50: 970–983.
120. Wang JH, Zuo XN, Gohel S, Milham MP, Biswal BB, et al. (2011) Graph theoretical analysis of functional brain networks: test-retest evaluation on short- and long-term resting-state functional MRI data. PLoS One 6: e21976.
121. Fox MD, Raichle ME (2007) Spontaneous fluctuations in brain activity observed with functional magnetic resonance imaging. Nat Rev Neurosci 8: 700–711.
122. Raichle ME, MacLeod AM, Snyder AZ, Powers WJ, Gusnard DA, et al. (2001) A default mode of brain function. Proc Natl Acad Sci U S A 98: 676–682.

doi:10.1093/scan/nst016 SCAN (2014) 9, 520–528

Altered orbitofrontal sulcogyral patterns in adult males with high-functioning autism spectrum disorders

Hiromi Watanabe,[1] Motoaki Nakamura,[1,2,3] Taisei Ohno,[1] Takashi Itahashi,[4] Eizaburo Tanaka,[1,5] Haruhisa Ohta,[1] Takashi Yamada,[1] Chieko Kanai,[1,3] Akira Iwanami,[1] Nobumasa Kato,[1,3] and Ryuichiro Hashimoto[1,3,6]

[1]Department of Psychiatry, Showa University School of Medicine, Tokyo, Japan, [2]Kinkou Hospital, Kanagawa Psychiatric Center, Kanagawa, Japan, [3]Japan Science and Technology Agency, CREST, Tokyo, Japan, [4]Department of Pharmacognosy and Phytochemistry, Showa University School of Medicine, Tokyo, Japan, [5]Department of Social Life Science, Nagoya University Graduate School of Medicine, Nagoya, Japan, and [6]Department of Language Sciences, Graduate School of Humanities, Tokyo Metropolitan University, Tokyo, Japan

Functions of the orbitofrontal cortex include diverse social, cognitive and affective processes, many of which are abnormal in autism spectrum disorders (ASDs). Recently, altered orbitofrontal sulcogyral patterns have been revealed in several psychiatric conditions, such as schizophrenia, indicating a possibility that altered orbitofrontal sulcogyral morphology reflects abnormal neurodevelopment. However, the presence of sulcal alterations in ASD remains unexplored. Using structural magnetic resonance imaging, subtypes of the 'H-shaped' sulcus (Type I, II and III, in order of frequency), posterior orbital sulcus (POS) and intermediate orbital sulcus were identified in each hemisphere of adult males with ASD ($n = 51$) and matched normal controls ($n = 55$) based on the study by Chiavaras and Petrides. ASD showed a significantly altered distribution of H-shaped sulcal subtypes in both hemispheres, with a significant increase of Type III. A significant alteration in the distribution of sulcal subtypes was also identified in the right hemisphere POS of ASD. Categorical regression analysis revealed that Type I and II expressions predicted a reduced total Autism-Spectrum Quotient score. Furthermore, Type I expression was associated with a reduced 'attention to detail' subscale score. The results demonstrate that altered sulcogyral morphology can be a marker for abnormal neurodevelopment leading to the increased risk of developing autism.

Keywords: autism spectrum disorder; magnetic resonance imaging; orbitofrontal cortex; brain sulcus; autistic trait

INTRODUCTION

Clinical symptoms of autism spectrum disorders (ASDs) can be characterized by marked impairments in socialization and communication along with restricted and repetitive behaviors (RRBs). Recent advances in clinical neuroscience have highlighted that deficits in a set of brain regions can be responsible for the impairments in social communicative functions and inflexible cognitive styles found in ASD. Among several regions, the importance of the orbitofrontal cortex (OFC) has been widely recognized (Baron-Cohen, 2002), particularly because of its key role in various facets of social cognition and behaviors (Schoenbaum and Roesch, 2005) as well as its dense connections to the amygdala and the anterior cingulate cortex, both of which are crucially involved in the pathophysiology of ASD (Barbas and Pandya, 1989; Ongur *et al.*, 2003). Despite its theoretical significance, empirical evidence for dysfunction of the OFC has not been consistently demonstrated by neuroimaging studies (Girgis *et al.*, 2007; Jiao *et al.*, 2010; Via *et al.*, 2011; Philip *et al.*, 2012). While several reasons for this lack of evidence can be considered, it is of note that there are technical difficulties specific to the OFC and its neighboring regions that hamper conventional magnetic resonance imaging (MRI) approaches; for example, large magnetic field inhomogeneity during functional MRI (Stenger, 2006).

For structural MRI studies, substantial interindividual variability in the sulcogyral pattern in the OFC can hamper interpretation of the volumetric measures derived by standard morphometric approaches, because definition of the region-of-interest (ROI) often relies on sulci in the manual drawing method, and variation of sulcogyral pattern could be a confounding factor at the spatial normalization step in the voxel-based morphometry (VBM). The development of the sulcogyral convolution is thought to reflect critical neurodevelopmental events, such as neuronal migration and local neuronal connection (Rakic, 1988; Armstrong *et al.*, 1995). Therefore, sulcogyral patterns may be significantly altered in neurodevelopmental disorders, which may further result in a systematic bias for structural measurements using VBM and manual ROI tracing methods.

Interindividual variability of the human orbitofrontal sulci has been systematically described in a seminal work using MR images of 100 hemispheres of 50 neurotypical individuals (Chiavaras and Petrides, 2000). Apart from the olfactory sulcus in the medial OFC, which is clearly visible and easily identifiable in every subject, the morphology of the other orbitofrontal sulci is highly complex and variable, and some sulci may not be consistently present between individuals. For instance, an 'H-shaped' sulcus refers to a configuration of multiple components of the medial orbital sulcus (MOS), lateral orbital sulcus (LOS) and transverse orbital sulcus (TOS). In a previous study by Chiavaras and Petrides, the H-shaped sulcus has been classified into three major subtypes (Type I, II and III, with Type I being the most common) based on the continuity of the MOS and LOS. A subsequent study reported an additional minor subtype (Type IV) that was found in 3–6% of the neurotypical population (Chakirova *et al.*, 2010). Pattern variations of the other orbitofrontal sulci have also been described, including the posterior orbital sulcus (POS) and the intermediate orbital sulcus (IOS), located in the posterior and anterior orbitofrontal gyri, respectively (Chiavaras and Petrides, 2000).

Several recent MRI studies have examined orbitofrontal sulcogyral variations in psychiatric populations. The sulcogyral formation is strongly regulated by genetic factors that mobilize sequences of early cortical folding developmental processes (Bartley *et al.*, 1997; Lohmann *et al.*, 1999), and after formation, sulcogyral morphology is thought to be stable throughout life (Armstrong *et al.*, 1995; Nakamura *et al.*,

Received 20 August 2012; Accepted 27 January 2013
Advance Access publication 5 February 2013
We thank Ms Matsushita and Saito for help with the collection of clinical and demographic data.
This work was supported by a Core Research for Evolutional Science and Technology (CREST) grant from Japan Science and Technology Agency to N.K. and by Grant-in-Aid for Scientific Research on Innovative Areas (23118003; Adolescent Mind and Self-Regulation) from the Ministry of Education, Culture, Sports, Science and Technology of Japan to R.H.

Correspondence should be addressed to Ryuichiro Hashimoto, PhD, Department of Psychiatry, Showa University School of Medicine, 6-11-11, Kita-karasuyama, Setagaya-ku, Tokyo 157-8577, Japan. E-mail: dbridges50@gmail.com

2007; Chakirova *et al.*, 2010). Although there is evidence that environmental and experiential factors later in life can modulate quantitative variables related to the sulcogyral folding, such as local gyrification index (Luders *et al.*, 2012), previous studies have identified series of critical events in early neural development that are thought to play central roles for determining cortical folding patterns [e.g. cortical growth (Toro and Burnod, 2005) and tensions from white matter fibers (Van Essen, 1997)], which led some researchers to propose that the sulcogyral pattern can be a morphological trait marker for psychiatric disorders with developmental origins (Nakamura *et al.*, 2007). Nakamura *et al.* (2007) were the first to report that the frequency distribution of H-shaped sulcus subtypes was significantly altered in schizophrenia, with an increased occurrence of Type III together with a reduced occurrence of Type I in the right hemisphere. This pattern of alteration was also observed in first-episode schizophrenic patients (Chakirova *et al.*, 2010; Takayanagi *et al.*, 2010) and individuals at high risk of developing schizophrenia (Chakirova *et al.*, 2010). Furthermore, Type III expression was associated with more severe psychotic symptoms and impulsivity in patients (Nakamura *et al.*, 2007) and higher ratings for psychosis in people at risk of developing schizophrenia (Chakirova *et al.*, 2010). These studies illustrate the possibility that the altered orbitofrontal sulcogyral pattern can indeed be a morphological trait marker for a psychiatric condition with neurodevelopmental aberration, predicting the development of particular clinical symptoms in later life.

This study examined the orbitofrontal sulcogyral morphology in adult males with high-functioning ASD. Given that ASD is a neurodevelopmental disorder with a strong genetic involvement (Muhle *et al.*, 2004; Sebat *et al.*, 2007), and that various aspects of social cognition and behavioral regulation functions of the OFC are impaired in ASD (Kringelbach and Rolls, 2004), we hypothesized that the frequency distribution of sulcal pattern variations would be significantly altered in ASD when compared with neurotypical individuals. Prediction of the specific pattern of alteration in the H-shaped sulcus is not straightforward from the results of previous studies of schizophrenia. However, if the increased expression of Type III in schizophrenia reflects neurodevelopmental abnormalities that commonly occur in other developmental disorders, we predict that Type III expression would be elevated in the ASD as well, perhaps in a more enhanced manner than schizophrenia. Furthermore, given the ample evidence of pathophysiological amygdala abnormalities in ASD (Lauvin *et al.*, 2012), it is possible that the POS pattern is also altered because the posterior OFC is considered part of the paralimbic region that has heavy anatomical connectivity with the amygdala. In addition, considering the morphological alterations in several neocortical association areas for social functions in ASD (e.g. inferior frontal gyrus), one might predict alteration of the IOS in the anterior OFC, which is also a part of neocortical association areas in the social brain network (Kringelbach and Rolls, 2004). Rather than focusing on a particular orbitofrontal sulcus, we systematically examined pattern variations in the H-shaped sulcus, POS and IOS separately, each of which has been shown to demonstrate substantial interindividual variability (Chiavaras and Petrides, 2000). Clinical correlation analyses of the OFC sulcogyral patterns were further performed to explore any relationship between orbitofrontal morphological traits and clinical features in ASD.

MATERIALS AND METHODS

Participants

Fifty-one adult males with ASD were recruited from outpatients at the Showa University Hospital. All patients were diagnosed with ASD based on the Diagnostic and Statistical Manual of Mental Disorders 4th Edition (DSM-IV) criteria and a medical chart review. A team of three experienced psychiatrists and a clinical psychologist performed the assessment. The assessment consisted of participant interviews about developmental history, present illness, life history and family history assessed independently by a psychiatrist and a clinical psychologist in the team. Participants were also asked to bring suitable informants who knew the participant in early childhood and about current mental or psychological symptoms, behavioral symptoms or motor skill deficits. At the end of the clinical interview, participants were formally diagnosed with pervasive developmental disorder by the psychiatrist if there was a consensus between the psychiatrists and the clinical psychologist. The diagnostic process required ~3 h. Patients with secondary autism related to a specific etiology such as tuberous sclerosis were excluded.

A group of 55 normal male controls (NC) were recruited by advertisements and acquaintances and screened using the Japanese version of the Mini-International Neuropsychiatric Interview (MINI) (Otsubo and Kamijima, 2000) by the same trained interviewers. No control subjects had an Axis-I psychiatric disorder or a first-degree relative with an Axis-I psychiatric disorder.

The intellectual ability was assessed using the Japanese version of the National Adult Reading Test (JART) (Nelson and Willison, 1991; Matsuoka and Kim, 2006). All subjects in both groups had an intelligent quotient (IQ) score > 80. Handedness was assessed using the Edinburgh Inventory of Handedness (Oldfield, 1971). To assess the presence and severity of autistic traits in each participant, the Autism-Spectrum Quotient (AQ) was administered (Baron-Cohen *et al.*, 2001). We used the Japanese version of the AQ, which has been assessed for its internal consistency reliability, test–retest reliability and discriminant validity (Kurita *et al.*, 2005; Wakabayashi *et al.*, 2006). To characterize autistic traits of each participant more specifically, we calculated the subscale scores of 'social interaction' and 'attention to detail' using the method proposed by Hoekstra *et al.* (2008).

Table 1 shows the demographic and clinical data of participants in the ASD and NC groups. Age, education and IQ were matched between the two groups (all $P > 0.15$). Handedness was significantly different ($P = 0.005$), consistent with several studies reporting an increased prevalence of left handedness in children with autism (Gillberg, 1983; Hauck and Dewey, 2001; Dane and Balci, 2007). At the time of the MRI scan, 11 of the 51 ASD participants were using the following medications: antidepressants (9 patients), anti-anxiety drugs (minor tranquilizer: 7 patients), hypnotic drugs (8 patients), antipsychotic drugs (4 patients) and antiepileptic drugs (1 patient). Most patients began taking medication only after reaching adolescence or adulthood (mean ± s.d.: 26.2 ± 9.2 years), which makes it unlikely that the medication can be a determinant factor of the sulcogyral patterns. Consistent with this view, Nakamura *et al.* (2007) reported that the OFC sulcogyral pattern was not associated with the antipsychotic dosage in patients with schizophrenia. All subjects participated in this study after providing written informed consent. This study was approved by the Ethics Committee of the Faculty of Medicine of Showa University.

MRI data acquisition

MR images were acquired on a 1.5-T General Electric Signa System (GE Medical Systems, Milwaukee, WI, USA) at the Karasuyama Hospital in Tokyo. In total, 128 contiguous sagittal images were collected from each individual using an eight-channel phased-array whole-head coil and a spoiled gradient-echo (SPGR) sequence with the following parameters: 25 ms repetition time; 5.2 ms echo time; flip angle = 20°; 24 × 24 cm field of view; 256 × 256 matrix and

Table 1 The demographic and clinical data for the participants

	ASD ($n = 51$)			NC ($n = 55$)			df	*t*-Value	*P*-value
	Mean	s.d.	Range	Mean	s.d.	Range			
Age (years)	30.9	8.2	19–51	32.0	7.1	19–49	104	0.676	0.501
Education (years)	15.3	2.1	9–21	14.6	2.0	12–18	85	1.41	0.161
Handedness	0.53	0.74	−1.00–1.00	0.90	0.32	−0.67–1.00	77	2.904	0.005[a]
ICV × 10^6 (mm^3)	1.6096	0.14931	1.1631–1.9910	1.6193	0.15150	1.1809–2.0910	104	0.33	0.743
Estimated IQ	109.8	9.5	89.5–119.8	107.1	9.0	87.5–119.8	94	1.44	0.152
AQ	35.5	5.3	24–47	14.3	5.8	3–30	95	18.84	<0.001[a]
Hoekstra's subscale									
Social interaction	121.8	11.7	96–144	82.0	12.1	52–106	95	16.44	<0.001[a]
Attention to detail	26.2	4.5	17–35	21.6	4.0	12–37	95	5.24	<0.001[a]

[a]Significant difference thresholded at $P = 0.01$.

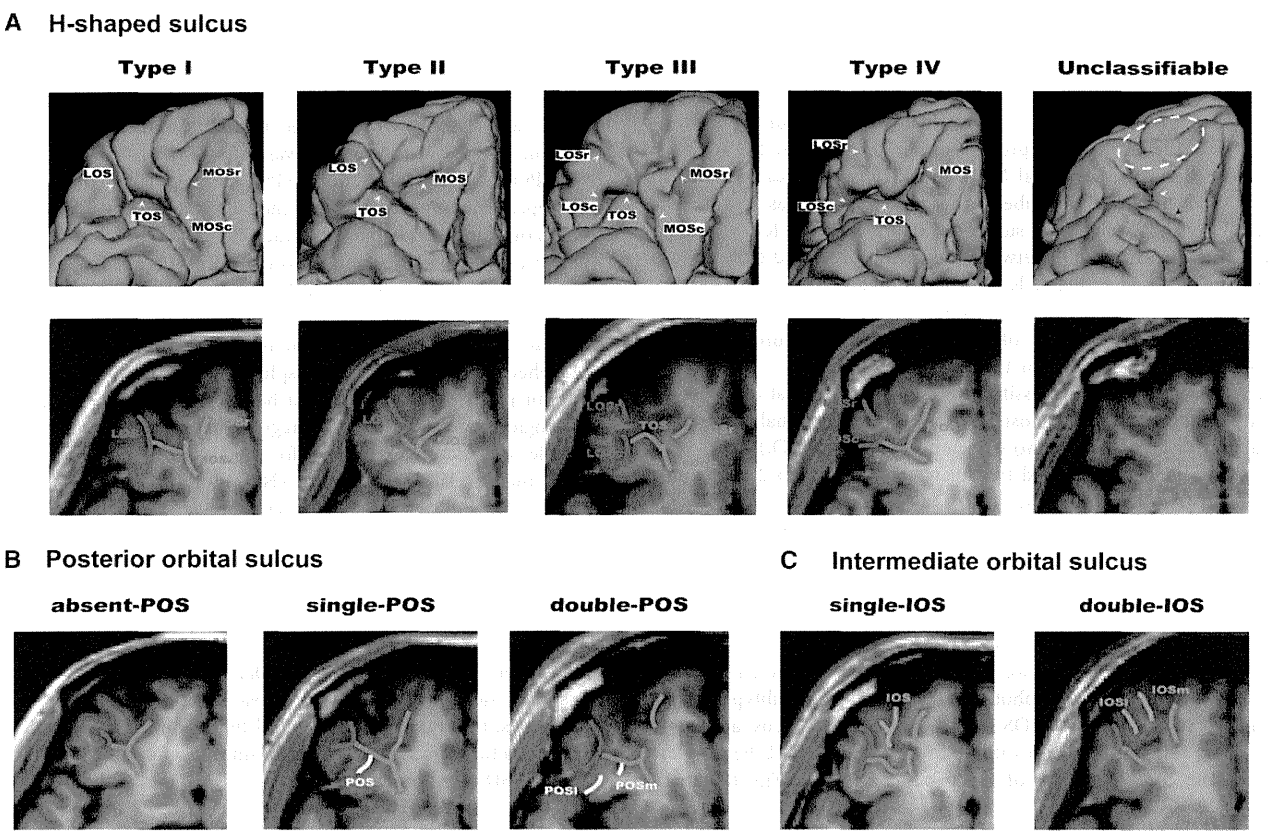

Fig. 1 Examples of the orbitofrontal sulcogyral patterns. (**A**) Variations of the H-shaped sulcus. Patterns were classified into four subtypes (Type I–IV) according to the continuity of the LOS and MOS in the rostrocaudal direction (r: rostral, c: caudal) (Type I: continuous LOS and discontinuous MOS, Type II: continuous LOS and MOS, Type III: discontinuous LOS and MOS, Type IV: discontinuous LOS and continuous MOS). The rightmost figure represents an ASD case that cannot be classified to either type using the classification systems of Chiavaras and Petrides (2000) and Chakirova *et al.* (2010). White dotted area shows clearly small and under-developed anterior orbital gyrus without any visible IOS. The TOS is not clearly identified (white arrow), and the caudal MOS and LOS are also unclear (black arrow). (**B**) Variants of the POS. The patterns were classified into three subtypes depending on the number of identified POS. (**C**) Variants of the IOS (m: medial, l: lateral). The patterns were classified into two subtypes depending on the number of identified IOS.

1.4 mm slice thickness. After acquisition, each image was resampled to 0.9375 × 0.9375 × 0.7 mm, and then realigned along the mid-sagittal anterior–posterior commissure line to correct any head tilt for consistent assessment of sulcogyral patterns.

Sulcogyral pattern identification

We classified sulcogyral pattern variations in the H-shaped sulcus (consisting of the TOS, MOS and LOS), POS and IOS into multiple subtypes in each hemisphere based on the previous description by Chiavaras and Petrides (2000) and a refined description for the H-shaped sulcus by Chakirova *et al.* (2010). In addition to the TOS, MOS, LOS, POS and IOS, we identified the neighboring olfactory sulcus and sulcus fragmentosus in each hemisphere to assist the precision and consistency of the sulcogyral classifications. We used three-dimensional slicer software (http://www.slicer.org/) to browse the SPGR images for visual identification of each orbitofrontal

sulcus. Freesurfer software (http://surfer.nmr.mgh.harvard.edu/) was also used to calculate the intracranial volume (ICV) of individual brains and to generate the pial and white matter surfaces that were used to assist the classification of sulcogyral subtypes.

The subtypes of the H-shaped sulci were identified on the basis of the continuity of the LOS and MOS in the rostrocaudal direction (Chiavaras and Petrides, 2000), as demonstrated in Figure 1A. In Type I, the rostral and caudal portions of the MOS were clearly interrupted, whereas the LOS was continuous throughout the entire length. In Type II, rostral and caudal portions of the MOS and LOS were continuous without interruption and were connected by the TOS. In Type III, rostral and caudal portions of both MOS and LOS were interrupted. In Type IV, the rostral and caudal portions of the LOS were interrupted in the presence of a continuous MOS, thus representing the opposite of Type I. The original work by Chiavaras and Petrides (2000) described only the first three subtypes, but Type IV was later identified in a small population of neurotypical individuals (Chakirova *et al.*, 2010). We included Type IV in our classification system to exhaust all four logical possibilities derived by continuity in both the LOS and MOS.

According to the previous study by Chiavaras and Petrides (2000), the POS can be either absent or present in the posterior orbital convexity in a hemisphere. If present, either one or two POS can be identified between the caudal MOS and LOS, which lies posterior to the TOS. In this study, we labeled these three variants as absent-POS, single-POS and double-POS subtypes (Figure 1B). The IOS was identified anterior to the TOS between the rostral MOS and LOS in both hemispheres in all individuals (Chiavaras and Petrides, 2000). Here, the IOS was classified into single-IOS and double-IOS subtypes depending on the number of identified sulci (Figure 1C) (see Supplementary material 1 for the detail).

The sulcogyral pattern classification in each individual was done by H.W., blinded to the diagnostic status of the individual. Inter-rater reliability was assessed by two clinicians (H.W. and T.O.), blinded to the diagnosis, who evaluated the sulcogyral patterns in 25 randomly selected participants. The intraclass correlation coefficients (Cronbach's α) were 0.958, 0.897 and 0.846 for the H-shaped sulcus, POS and IOS, respectively.

Statistical analysis

We used SPSS software (version 18.0, SPSS, Chicago, IL, USA) for statistical analysis. Initially, we assessed differences between the ASD and NC groups in the distribution of the sulcogyral subtypes of the H-shaped sulcus, POS and IOS separately. For each sulcus, a separate chi-square test was applied to the frequency data in each hemisphere and to the combined data of the two hemispheres. The frequency distribution observed in the NC group was used as the expected number for each subtype. After examining group differences in the frequency distributions between the ASD and NC groups of our data, we also performed the same statistical tests using the frequency data of our NC group and that described by Chiavaras and Petrides (2000) to check the validity of our data. Only Type I, II and III data were used to analyze the H-shaped sulcus because the Type IV classification only occurred in 6 of 212 hemispheres (2.8%; Table 1), providing insufficient data to perform any reliable group comparison.

We then performed categorical regression analysis to determine which variations of the OFC sulci predict autistic traits. Categorical regression analysis was selected, because this model allows us to examine the effects of multiple factors (i.e. sulcogyral subtypes) in a single integrated model without using multiple independent statistical tests (Nakamura *et al.*, 2007, 2008; Roppongi *et al.*, 2010; Uehara-Aoyama *et al.*, 2011). Each individual participant was classified according to whether he possessed the H-shaped sulcus (Type I, II and III) or POS (absent, single and double), subtypes in either hemisphere. In this analysis, the IOS subtypes were not included because the frequency distribution was comparable between the ASD and NC groups (see 'Results' section), and were therefore unlikely to predict autistic traits. The classification resulted in six nominal variables (Type I, Type II, Type III, absent POS, single POS and double POS), each of which was entered as an independent variable in a single model of categorical analysis regression. In our categorical regression, each categorical predictor represents whether a particular participant has the sulcal subtype (represented by that predictor) in the left or right hemisphere. This means that, in the Type I predictor, for example, we put a categorical value for participants who had Type I either in the left hemisphere only, or in the right hemisphere only, or in both hemispheres. In contrast, we put another value for participants who did not have Type I in either hemisphere. The single model of categorical regression was adopted rather than multiple univariate comparisons for the six independent variables to reduce the risk of false positives (Nakamura *et al.*, 2007). Separate models were built to predict dependent variables of the total AQ score (Baron-Cohen *et al.*, 2001), 'social interaction' and 'attention to detail' subscale scores individually (Hoekstra *et al.*, 2008). Three other models consisting of the same six nominal variables were also built for handedness, estimated IQ scores and ICVs. The odds ratio was calculated by cross-tabulation using SPSS to estimate the risk of developing ASD from expression of particular sulcogyral subtypes. The cross-tabulation consisted of three variables of the left H-shaped sulcal types, the right H-shaped sulcal types and the right POS types, all of which turned out to show significant frequency difference between NC and ASD (see 'Results' section).

Table 2 Distributions of orbitofrontal sulcal patterns of the ASD and NC in this study and NC in Chakirova and Petrides (2000)

	H-shaped sulcus *N* (%)				IOS *N* (%)		POS *N* (%)		
	I	II	III	IV	Single	Double	Absent	Single	Double
ASD									
Left	26 (52)	12 (24)	12 (24)	0 (0)	42 (84)	8 (16)	11 (22)	33 (66)	6 (12)
Right	23 (46)	15 (30)	10 (20)	2 (4)	33 (66)	17 (34)	21 (42)	26 (52)	3 (6)
Total (left + right)	49 (49)	27 (27)	22 (22)	2 (2)	75 (75)	25 (25)	32 (32)	59 (59)	9 (9)
NC									
Left	27 (49)	19 (35)	6 (11)	3 (5)	44 (80)	11 (20)	10 (18)	36 (66)	9 (16)
Right	35 (63)	13 (24)	6 (11)	1 (2)	41 (75)	14 (25)	14 (26)	37 (67)	4 (7)
Total (left + right)	62 (56)	32 (29)	12 (11)	4 (4)	85 (77)	25 (23)	24 (22)	73 (66)	13 (12)
NC in Chiavaras and Petrides (2000)									
Left	24 (48)	17 (34)	9 (18)	0 (0)	41 (82)	9 (18)	12 (24)	28 (56)	10 (20)
Right	32 (64)	13 (26)	5 (10)	0 (0)	40 (80)	10 (20)	11 (22)	34 (68)	5 (10)
Total (left + right)	56 (56)	30 (30)	14 (14)	0 (0)	81 (81)	19 (19)	23 (23)	62 (62)	15 (15)

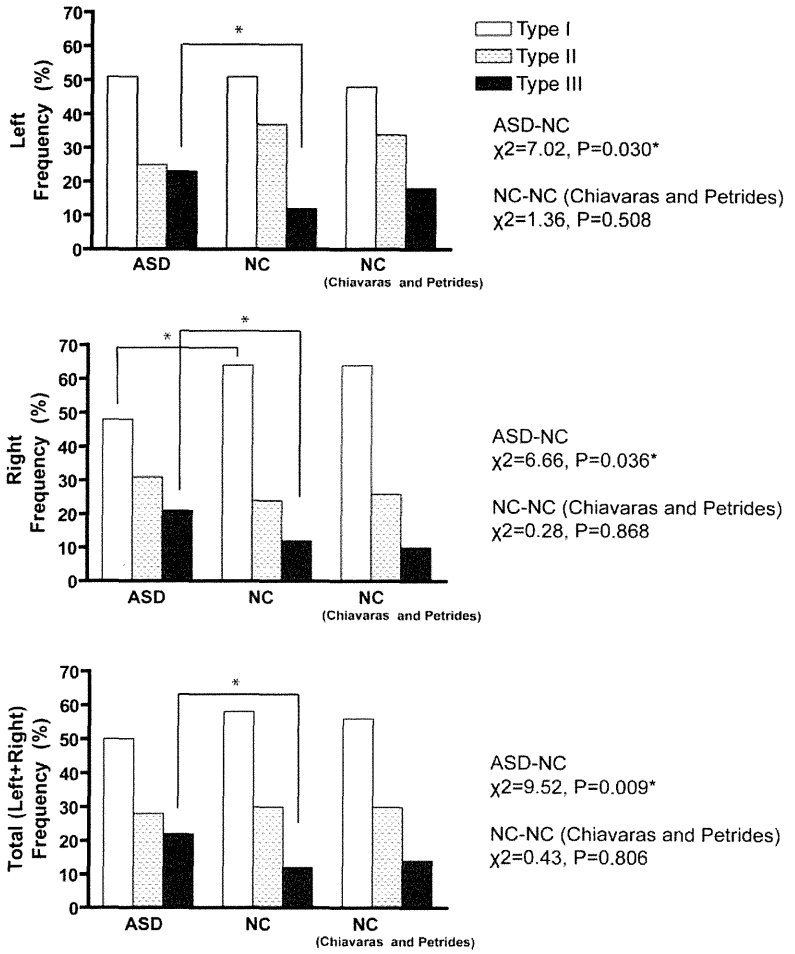

Fig. 2 Sulcal pattern distribution of the 'H-shaped' sulcus in the OFC. Right column shows results from the previous study on neurotypical individuals by Chiavaras and Petrides (2000). According to *post hoc* test, Type III expression was increased in both hemispheres in the ASD group compared with the NC group (left: $\chi^2 = 5.75$, $P = 0.016$, right: $\chi^2 = 3.80$, $P = 0.051$, bilateral: $\chi 2 = 9.45$, $P = 0.002$), whereas Type I expression was deceased in the right hemisphere ($\chi 2 = 5.93$, $P = 0.015$). *Significant difference thresholded at $P = 0.05$.

RESULTS

Sulcogyral pattern distribution

Table 2 shows the frequency of the H-shaped sulcus, POS and IOS subtypes in each group. One ASD patient displayed a highly unusual sulcogyral pattern in which rostral components of the H-shaped sulcus were absent or immature in both hemispheres (Figure 1A). In this case, the rostral side of the OFC was extremely small in both hemispheres; therefore, IOS could not be identified. Figure 2 shows the distribution of the H-shaped sulcal subtypes excluding this case and cases showing Type IV (see 'Materials and methods' section). The distributions of the POS and IOS subtypes are shown in Figures 3 and 4, respectively.

We found a significant group difference in the distribution of subtypes of the H-shaped sulcus in both hemispheres (Figure 2). *Post hoc* tests revealed that occurrence of Type III was greater in both hemispheres in the ASD group compared with the NC group, whereas expression of Type I was deceased in the right hemisphere. We confirmed that the distribution of the H-shaped sulcal subtypes in the NC group was consistent with that of the previous study (Chiavaras and Petrides, 2000).

The distribution of the POS subtypes in the ASD group was significantly different from that in the NC group in the right hemisphere and in the combined data of the two hemispheres (Figure 3). *Post hoc* tests showed a significant increase in the occurrence of the absent-POS subtype and a decrease in the occurrence of the single-POS subtype in the right hemisphere in the ASD group. The distributions of the IOS subtypes were not significantly different between the two groups (Figure 4). The distributions of the POS and IOS subtypes in the NC group were comparable with those reported by Chiavaras (Figures 3 and 4).

The odds ratio calculated by the cross-tabulation showed that, compared to subjects without Type III occurrence, participants with Type III expression in any hemisphere showed a 2.67-fold increase in morbid risk for ASD, and that, compared to those with either single POS or double POS in the right hemisphere, participants with the absent-POS subtype in the right hemisphere showed a 1.40-fold increase in morbid risk. Moreover, compared to participants without Type III expression in both hemispheres and absent POS in the right hemisphere, participants with Type III occurrence in any hemisphere combined with absent-POS subtype in the right hemisphere showed a 4.89-fold increase in morbid risk for ASD.

Categorical regression analysis of OFC sulcogyral patterns

Categorical regression analysis revealed that, within the ASD group, expressions of Type I and II were significantly associated

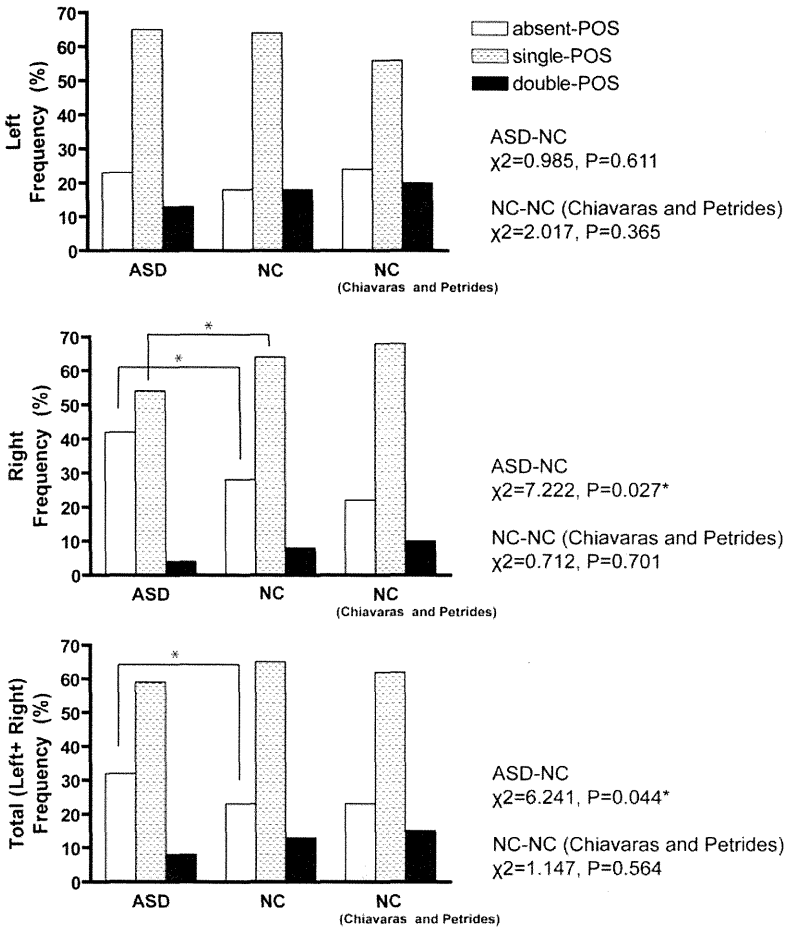

Fig. 3 Sulcal pattern distribution of the POS in the OFC. Right column shows results from Chiavaras and Petrides (2000). *Post hoc* tests showed significant increase of the absent POS in the right hemisphere ($\chi^2 = 7.213$, $P = 0.007$) and bilateral hemispheres ($\chi^2 = 6.078$, $P = 0.014$), and decrease of the 'single POS' in the right hemisphere ($\chi^2 = 5.297$, $P = 0.021$). *Significant difference thresholded at $P = 0.05$.

with reduced total AQ scores (Table 3). Moreover, Type I expression was also associated with reduced scores on the 'attention to detail' subscale. Type III expression or any of the POS subtypes was not significantly associated with either the total AQ score or the two subscales (Table 3).

Within the NC group, no significant association between a particular sulcal subtype and AQ score was found (Table 3). Categorical regression analysis showed no significant association of sulcogyral subtypes either with handedness [ASD: $F(6,41) = 1.315$, $P = 0.276$; NC: $F(6,36) = 1.306$, $P = 0.285$], ICV [ASD: $F(6,47) = 1.992$, $P = 0.089$; NC: $F(6,50) = 0.669$, $P = 0.675$] or estimated IQ [ASD: $F(6,42) = 0.539$, $P = 0.775$; NC: $F(6,45) = 1.225$, $P = 0.315$].

DISCUSSION

To our knowledge, this study is the first to reveal altered distributions of the orbitofrontal sulcogyral patterns in individuals with high-functioning ASD. Whereas previous psychiatric studies targeted only one of the three orbitofrontal sulci (Nakamura *et al.*, 2007; Chakirova *et al.*, 2010; Roppongi *et al.*, 2010; Takayanagi *et al.*, 2010; Uehara-Aoyama *et al.*, 2011), we performed an extended study on all three sulci that have been shown to display major interindividual variability within the OFC (Chiavaras and Petrides, 2000). For the H-shaped sulcus, the frequency distribution of sulcal subtypes in ASD was significantly altered from that in the NC group in both hemispheres: Type III expression was increased in both hemispheres together with reduced occurrence of Type I in the right hemisphere. Furthermore, in ASD, the absent-POS subtype occurred significantly more frequently, combined with reduced frequency of the single-POS subtype in the right hemisphere. No significant group difference was found for the IOS. Subsequent categorical regression analysis for predicting autistic traits indicated that expressions of Type I and II in the H-shaped sulcus were associated with reduced total AQ score. More specifically, the occurrence of Type I was associated with a decreased subscale score for 'attention to detail'. These findings have demonstrated altered expressions of the orbitofrontal sulcogyral morphology in individuals with ASD that may predict the severity of general and specific autistic traits.

Variations of the H-shaped sulcal pattern

Altered distribution of sulcal subtypes in ASD was most clearly demonstrated for the H-shaped sulcus in both hemispheres. More specifically, increased expression of Type III was observed in both hemispheres. Compared with other subtypes, the morphology of Type III may be characterized as less mature development of the sulcogyral formation. According to previous research on the development of the human infant brain (Chi and Dooling, 1976; Dubois *et al.*, 2008; Habas *et al.*, 2012), the formation of the orbitofrontal sulcogyral patterns can be identified between 16 and 44 weeks of gestation, starting from the posteromedial region and then extending along the anterior and lateral directions (Kringelbach and Rolls, 2004). Future